

REFINING THE CENSUS OF THE UPPER SCORPIUS ASSOCIATION WITH *GAIA*¹

K. L. LUHMAN^{2,3} AND T. L. ESPLIN^{4,5}

Draft version May 21, 2020

ABSTRACT

We have refined the census of stars and brown dwarfs in the Upper Sco association (~ 10 Myr, ~ 145 pc) by 1) updating the selection of candidate members from our previous survey to include the high-precision astrometry from the second data release of *Gaia*, 2) obtaining spectra of a few hundred candidate members to measure their spectral types and verify their youth, and 3) assessing the membership (largely with *Gaia* astrometry) of 2020 stars toward Upper Sco that show evidence of youth in this work and previous studies. We arrive at a catalog of 1761 objects that are adopted as members of Upper Sco. The distribution of spectral types among the adopted members is similar to those in other nearby star-forming regions, indicating a similar initial mass function. In previous studies, we have compiled mid-infrared photometry from *WISE* and the *Spitzer Space Telescope* for members of Upper Sco and used those data to identify the stars that show evidence of circumstellar disks; we present the same analysis for our new catalog of members. As in earlier work, we find that the fraction of members with disks increases with lower stellar masses, ranging from $\lesssim 10\%$ for $> 1 M_{\odot}$ to $\sim 22\%$ for $0.01\text{--}0.3 M_{\odot}$. Finally, we have estimated the relative ages of Upper Sco and other young associations using their sequences of low-mass stars in $M_{G_{\text{RP}}}$ versus $G_{\text{BP}} - G_{\text{RP}}$. This comparison indicates that Upper Sco is a factor of two younger than the β Pic association (21–24 Myr) according to both non-magnetic and magnetic evolutionary models.

Subject headings: brown dwarfs — stars: formation — stars: low-mass — stars: luminosity function, mass function — stars: pre-main sequence

1. INTRODUCTION

The Upper Scorpius subgroup in the Scorpius-Centaurus OB association (Sco-Cen) contains one of the largest nearby populations of newly-formed stars ($d \sim 145$ pc, $\tau \sim 10$ Myr, Preibisch & Mamajek 2008). Since it extends across a large area of sky (~ 100 deg²), a census of its members requires wide-field imaging data. The extinction in Upper Sco is low enough ($A_V < 3$ mag) that it has been possible to perform wide-field surveys of the association across a broad range of wavelengths (e.g., Preibisch et al. 1998; Lodieu et al. 2006; Slesnick et al. 2006; Rizzuto et al. 2015; Pecaute & Mamajek 2016). Luhman et al. (2018) compiled stars within the confines of Upper Sco that have spectral classifications and evidence of youth and whose available measurements of proper motion and parallax are consistent with membership, resulting in a catalog of more than 1600 proposed members. That study also presented ~ 1200 additional candidate members that lacked spectroscopy.

Luhman et al. (2018) utilized data from several surveys, including the first data release (DR1) from the *Gaia* mission (Perryman et al. 2001; de Bruijne 2012; Gaia

Collaboration et al. 2016b), which provided an all-sky catalog of high-precision proper motions and parallaxes for stars with $G \lesssim 12$ mag (Gaia Collaboration et al. 2016a). Since Luhman et al. (2018), the second data release of *Gaia* (DR2) has been issued, which has extended measurements of those parameters down to much fainter magnitudes ($G \sim 20$ mag, Gaia Collaboration et al. 2018b). Data from DR1 and DR2 have been applied extensively to young clusters and association for the measurement of the distances and internal kinematics of known members (Dzib et al. 2018; Galli et al. 2018; Roccatagliata et al. 2018; Wright & Mamajek 2018; Wright et al. 2019; Kuhn et al. 2019) and for the identification of candidate members (Cook et al. 2017; Oh et al. 2017; Beccari et al. 2018; Wilkinson et al. 2018; Gagné et al. 2018; Gagné & Faherty 2018; Faherty et al. 2018; Luhman 2018; Röser et al. 2018; Herczeg et al. 2019; Galli et al. 2020). The DR2 magnitude limit for parallaxes and proper motion corresponds to especially low masses in Upper Sco ($\sim 0.04 M_{\odot}$) due to the combination of its proximity, low extinction, and youth. Indeed, DR2 has been used to identify candidate members of Upper Sco and other populations in Sco-Cen and to examine spatial and kinematic substructure among those candidates (Goldman et al. 2018; Cánovas et al. 2019; Damiani et al. 2019).

We have sought to further improve the census of Upper Sco using data from *Gaia* DR2 and new spectroscopy of candidate members. We begin by using *Gaia* data to characterize the kinematics of the stellar populations within Sco-Cen and to define kinematic criteria for membership in Upper Sco (Section 2). Those criteria are incorporated into the selection of candidate members of Upper Sco from Luhman et al. (2018) and spectral clas-

¹ Based on observations made with the Two Micron All Sky Survey, the *Gaia* mission, the NASA Infrared Telescope Facility, Cerro Tololo Inter-American Observatory, Gemini Observatory, the Magellan Baade Telescope at Las Campanas Observatory, and the Bok Reflector at Steward Observatory.

² Department of Astronomy and Astrophysics, The Pennsylvania State University, University Park, PA 16802, USA; kll207@psu.edu

³ Center for Exoplanets and Habitable Worlds, The Pennsylvania State University, University Park, PA 16802, USA

⁴ Steward Observatory, University of Arizona, 933 North Cherry Avenue, Tucson, AZ 85721, USA

⁵ Strittmatter Fellow.

sifications are presented for a few hundred candidates (Section 3). We compile a catalog of stars toward Upper Sco that exhibit spectroscopic evidence of youth and assess their membership in the association (Section 4). Using the adopted members and the most promising remaining candidates that lack spectra (i.e., those with *Gaia* astrometry), we characterize the stellar population of Upper Sco in terms of its initial mass function (IMF), disk fraction, and median age (Section 5). An appendix also includes comments on individual sources, extinction coefficients in the *Gaia* bands based on the extinction curve from Schlafly et al. (2016), and new estimates for the typical intrinsic colors of young stellar photospheres in optical and infrared (IR) bands.

2. KINEMATIC MEMBERSHIP CRITERIA FOR UPPER SCO

2.1. *Gaia* DR2

To improve upon the recent census of Upper Sco from Luhman et al. (2018), we make use of new data from *Gaia* DR2. They include photometry in bands at 3300–10500 Å (G), 3300–6800 Å (G_{BP}), and 6300–10500 Å (G_{RP}), proper motions and parallaxes for most stars down to $G \sim 20$ mag, and radial velocities primarily for $G \sim 4$ –12 mag. The additional contents of DR2 are summarized by *Gaia* Collaboration et al. (2018b).

DR2 contains parameters that can be used to identify stars with poor astrometric fits, and hence potentially unreliable astrometry (*Gaia* Collaboration et al. 2018c). After DR2, Lindegren (2018) defined a new parameter to serve as a better indicator of the goodness of fit, the renormalized unit weight error (RUWE). The distribution of RUWE in DR2 exhibited a maximum centered near unity (well-behaved fits) and a long tail at values higher than ~ 1.4 . Therefore, Lindegren (2018) suggested that $\text{RUWE} \lesssim 1.4$ could be used as a threshold for reliable astrometry. Esplin & Luhman (2019) examined the applicability of that threshold to the Taurus star-forming region, and found that a break does appear near that value in the distribution of RUWE for the known members. The fraction of members with discrepant astrometry increased with larger values of RUWE above 1.4, although many members above that threshold had astrometry that was consistent with membership, and thus did not appear to have large errors. We have repeated that exercise for Upper Sco in Figure 1, where we plot the distribution of $\log(\text{RUWE})$ for the members adopted by Luhman et al. (2018). The population of well-behaved fits near unity is slightly broader in Upper Sco than in Taurus, so we adopt a larger threshold ($\text{RUWE} < 1.6$) when selecting reliable astrometry for our analysis. As with Taurus, many of the previously adopted members of Upper Sco with high values of RUWE have astrometry that is consistent with membership.

2.2. Kinematics in Sco-Cen

As often done in surveys for new members of clusters and associations, Luhman et al. (2018) used previously known young stars in the direction of Upper Sco to define photometric and kinematic criteria for the selection of new candidate members. However, because Upper Sco is one of several populations within the Sco-Cen complex, some of which overlap on the sky, we examine the kinematics of the entire complex in order to identify those

that apply to Upper Sco. To reveal the kinematics of the various populations in Sco-Cen, we begin by identifying a sample of candidate young stars using a color-magnitude diagram (CMD). In Figure 2, we plot $M_{G_{RP}}$ versus $G_{BP} - G_{RP}$ for stars from DR2 that are within the boundary of Sco-Cen from de Zeeuw et al. (1999), are close enough to be members of the complex ($\pi > 5$ mas), and have small relative errors in parallax ($\pi/\sigma \geq 20$) and reliable astrometry ($\text{RUWE} < 1.6$). The threshold in π/σ was chosen to be high enough that measurement errors in parallax and proper motion are a negligible component of the spread in those parameters in Sco-Cen while low enough to produce a sufficiently large sample of stars for fully sampling the kinematics of Sco-Cen. We have selected a sample of candidate young low-mass stars based on colors between $G_{BP} - G_{RP} = 1.4$ –3.4 mag ($\sim K5$ – $M5$, ~ 0.15 – $1 M_{\odot}$) and absolute magnitudes above the single-star sequence for the Tuc-Hor association (45 Myr, Bell et al. 2015), which is older than the oldest isochronal ages for known members of Sco-Cen ($\lesssim 30$ Myr, Pecaut et al. 2012; Pecaut & Mamajek 2016).

In Figure 3, we have plotted the proper motions ($\mu_{\alpha,\delta}$) and proper motion offsets ($\Delta\mu_{\alpha,\delta}$) from *Gaia* DR2 for the candidate young stars identified with the CMD in Figure 2. The proper motion offset is defined as the difference between the observed proper motion for a given star and the motion expected at the star’s celestial coordinates and parallax if it had the median space velocity of members of Upper Sco from Luhman et al. (2018) rounded to the nearest integers ($U, V, W = -5, -16, -7$ km s $^{-1}$, see also Section 4). Stars with the same space velocities but different celestial coordinates exhibit different proper motions. The proper motion offsets serve to reduce those projection effects, which is why the candidate young stars in Figure 3 are more tightly clustered in those parameters. The smaller concentration of proper motion offsets corresponds to the open cluster IC 2602, which has an age of 46 Myr (Dobbie et al. 2010). The larger group of offsets contains the populations in Sco-Cen.

To include parallax in our kinematic analysis of Sco-Cen, we have plotted $\Delta\mu_{\alpha}$ and $\Delta\mu_{\delta}$ versus parallax in the top row of Figure 4 for the candidate young stars from Figure 2. These data exhibit a rich, complex distribution and a sparse, widely scattered distribution, which correspond to Sco-Cen and field stars, respectively. Many of these candidate members of Sco-Cen have been previously identified with *Gaia* DR2 (Goldman et al. 2018; Cánovas et al. 2019; Damiani et al. 2019). We have estimated probabilities of membership in Sco-Cen and the field population by applying a Gaussian mixture model to the parallaxes and proper motion offsets using the `mclust` package in R (R Core Team 2013; Scrucca et al. 2016). The mixture model included a noise component for the field stars, which was initialized using the nearest neighbor cleaning method from Byers & Raftery (1998) via the `NNclean` function in the `prabcus` library of R. Fits were performed with models in which the number of components ranged from 1 to ~ 20 . We have adopted the model with the smallest number of components that is effective at discriminating between the field stars and members of Sco-Cen based on the distributions of membership probabilities, which corresponds to the model

with three components for Sco-Cen. In that model, most stars ($\sim 95\%$) have a high probability ($>90\%$) of membership in either Sco-Cen or the field population. That fraction does not increase significantly for models with more than three components. We note that the Gaussian mixture model applied by `mclust` does not make use of measurement errors. However, the errors in parallaxes and proper motion offsets for the sample in question are much smaller than the ranges of values in Sco-Cen, so the identification of populations and the estimates of membership probabilities should not depend significantly on the inclusion of those errors.

The parallaxes and proper motion offsets for the 5353 stars with $>90\%$ probabilities of membership in Sco-Cen are plotted in the bottom row of Figure 4. We have included an ellipse (2σ) for each of the three components in the model. A map of those stars is presented in Figure 5. We have marked the boundaries for the three subgroups of Sco-Cen from de Zeeuw et al. (1999), which consist of Upper Sco, Upper Centaurus-Lupus (UCL) and Lower Centaurus-Crux (LCC). We also have included the boundary between Upper Sco and the Ophiuchus star-forming region that was adopted by Esplin et al. (2018) and rectangles that encompass clouds 1–4 in the Lupus star-forming region. In Figure 5, the densest concentrations of stars are found in Upper Sco and in a cluster associated with V1062 Sco (Röser et al. 2018; Damiani et al. 2019). The remaining stars are more widely scattered across the subgroups of Sco-Cen. The three components of our adopted mixture model correspond primarily to Upper Sco/Ophiuchus/Lupus, the V1062 Sco cluster, and UCL/LCC, as indicated in Figure 4.

The variation of kinematics across Sco-Cen is illustrated in Figure 6, which shows the parallaxes and proper motion offsets for the candidate members from Figure 5 that within the boundaries of each of the three subgroups. The broadest population in parallax from our mixture model is concentrated within the boundaries of UCL and LCC, but it extends across Upper Sco as well. That population exhibits a shift in parallax and $\Delta\mu_\alpha$ between UCL and LCC. To better isolate the kinematics of Upper Sco and Ophiuchus, we have used the functions `kde2d` and `bandwidth.nrd` from the `MASS` package in R (Venables & Ripley 2002) to calculate density maps in $(\pi, \Delta\mu_\alpha)$ and $(\pi, \Delta\mu_\delta)$ for the Sco-Cen members within the boundary of Ophiuchus from Esplin et al. (2018) and for members outside of that boundary and within the triangular area in which most Upper Sco members are concentrated (Fig. 5). The latter region is referred to as the “central concentration” of Upper Sco henceforth in this study. Contours for the resulting density maps are plotted in Figure 6, which show a shift in the kinematics between the two populations (see also Damiani et al. 2019). For the purpose of assessing membership in Upper Sco and Ophiuchus in Section 4.1, we have adopted thresholds in parallax, $\Delta\mu_\alpha$, and $\Delta\mu_\delta$ that approximate the 10% contours for the two populations in Figure 6. In a similar way, we have also defined thresholds for membership in UCL/LCC that follow the outer contours of a density map for the sum of the UCL and LCC samples in Figure 6. We note that young stars associated with the Lupus clouds (Comeron 2008, references therein) are similar to Upper Sco in their proper motion offsets but are slightly more distant with a median parallax of ~ 6.3 mas.

Since our Gaussian mixture model was applied only to parallax and proper motion offsets, it is possible for members of a given population to be widely separated on the sky. For instance, the diagrams in Figure 6 for LCC contain several stars that have kinematics similar to the V1062 Sco cluster, which is more than 30° from LCC. Given the compact nature of V1062 Sco, it seems likely that those stars are unrelated to V1062 Sco or Sco-Cen. We have investigated mixture models that include celestial coordinates, but the resulting populations were less satisfactory because of the non-Gaussian distributions of positions of young stars across UCL and LCC.

We have compared the sample of 5353 stars with $>90\%$ membership probabilities in Sco-Cen from our Gaussian mixture model to the sample of 10,839 candidate members identified with *Gaia* DR2 by Damiani et al. (2019). We find that 5295 of our candidates (99%) are also in the sample from Damiani et al. (2019). Among the 5544 candidates from Damiani et al. (2019) that are absent from our sample, 4713 are candidate members of IC 2602 (which we ignored) or are outside of the ranges of values that we considered for celestial coordinates, $G_{BP} - G_{RP}$, or RUWE. An additional 200 of those 5544 candidates appear below the boundary in Figure 2 that we used for identifying young stars. The remaining 631 candidates from Damiani et al. (2019) that are absent from our sample have low probabilities of membership in the three components of our Gaussian mixture model that correspond to Sco-Cen. Those stars have proper motion offsets and parallaxes in Figure 6 that differ significantly from the three Sco-Cen components, so they were assigned to the noise component (field stars) by our model.

3. SEARCH FOR NEW MEMBERS OF UPPER SCO

3.1. Application of *Gaia* DR2

Using CMDs, proper motions, and parallaxes (when available), Luhman et al. (2018) identified candidate members of Upper Sco within the area from $\alpha = 15^{\text{h}}35^{\text{m}}$ to $16^{\text{h}}45^{\text{m}}$ and $\delta = -30$ to -16° and outside of the boundary of Ophiuchus defined by Esplin et al. (2018). They considered astrometry and photometry from the Point Source Catalog of the Two Micron All Sky Survey (2MASS, Skrutskie et al. 2006), the third data release of the Deep Near-Infrared Survey of the Southern Sky (Epchtein et al. 1999), the science verification release and data release 10 (DR10) of the United Kingdom Infrared Telescope Infrared Deep Sky Survey (UKIDSS, Lawrence et al. 2007), the AllWISE Source Catalog of the *Wide-field Infrared Survey Explorer* (*WISE*, Wright et al. 2010), the first data release of the 3π survey from Pan-STARRS1 (PS1, Kaiser et al. 2002, 2010; Chambers et al. 2016; Flewelling et al. 2016), DR1 from *Gaia* (Gaia Collaboration et al. 2016a), and the fifth data release of the Visible and Infrared Survey Telescope for Astronomy (VISTA) Hemisphere Survey (VHS, McMahon et al. 2013). Luhman et al. (2018) presented a catalog of 1196 candidate members of Upper Sco that were identified with those data and that lacked spectroscopic confirmation of their youth. In this study, we have updated the VHS photometry in our candidate selection with data from the sixth data release (DR6). In terms of *JHK* photometry, UKIDSS and VHS exhibit a systematic offset from 2MASS that varies with color, and

hence spectral type, due to differences in the transmission profiles of their filters (Hodgkin et al. 2009). We have applied offsets to the UKIDSS and VHS data to align them with the 2MASS data, on average, for the known M-type members of Upper Sco (most members at earlier types are saturated in UKIDSS and VHS), which corresponds to adding 0.07, -0.04 , and 0.03 mag to J , H , and K from UKIDSS and adding 0.07 and -0.03 mag to J and K from VHS, respectively. These offsets were not included in the analysis from Luhman et al. (2018).

To further refine the sample of candidates from Luhman et al. (2018), we can employ the kinematic criteria for membership from the previous section (Figure 6) using *Gaia* DR2. We identified those criteria by considering stars with sufficiently precise astrometry ($\pi/\sigma \geq 20$) that we could accurately characterize the kinematics of Upper Sco. We now apply those criteria to a broader range of parallax errors ($\pi/\sigma \geq 10$) when identifying candidate members of Upper Sco. Data from DR2 are available for 1095 of the 1196 candidates, 972 of which have $\pi/\sigma \geq 10$. Among the stars with $\pi/\sigma \geq 10$ and reliable astrometry as indicated by $\text{RUWE} < 1.6$ (Section 2.1), we have rejected those that do not overlap (at 1σ)⁶ with the ranges of parallax and proper motion offsets for the central concentration of Upper Sco in Figure 6, which results in the rejection of 370 candidates. For stars with $\text{RUWE} > 1.6$, agreement with those criteria is taken as additional evidence supporting candidacy and disagreement is ignored and does not affect candidacy. For stars that lack precise parallaxes but that have single-epoch positions from DR2, we have replaced the 2MASS/*Gaia* DR1 proper motions from Luhman et al. (2018) with new measurements using 2MASS and the DR2 positions. Those updated proper motions lead to the rejection of four candidates. Following our new adjustments to the UKIDSS and VHS photometry described earlier in this section, 20 additional candidates from Luhman et al. (2018) no longer satisfy the selection criteria in the CMDs from that study. Thus, a total of 394 candidates from Luhman et al. (2018) are now rejected.

Since many of the proper motion measurements employed by Luhman et al. (2018) are superseded by more accurate data from *Gaia* DR2 or 2MASS/*Gaia* DR2, some stars that were rejected in that study now qualify as candidate members. In addition, stars with $\pi/\sigma \geq 10$ and $\text{RUWE} < 1.6$ are adopted as candidates if they satisfy the kinematic criteria for membership from the previous section, appear above the single-star sequence for the Tuc-Hor association in a diagram of $M_{G_{\text{RP}}}$ versus $G_{\text{BP}} - G_{\text{RP}}$ (Figure 2), and are not previously identified members or candidates. These candidates consist of stars that were rejected by a few of the CMDs from Luhman et al. (2018) or lacked sufficient photometry to be selected as candidates in that study because they are close companions or bright stars that are absent from the 2MASS Point Source Catalog. We also selected stars that have $\pi/\sigma \geq 10$, satisfy the kinematic criteria in Figure 6, lack photometry in G_{BP} or G_{RP} , and are within $5''$ of a candidate or known member. Finally, some stars that were rejected by CMDs in Luhman et al. (2018) now

satisfy those diagrams because of the new offsets applied to the photometry from UKIDSS and VHS. In total, we have identified 155 candidate members of Upper Sco that were not in the catalog of candidates from Luhman et al. (2018).

We have rejected 394 of the 1196 candidate members of Upper Sco from Luhman et al. (2018) and have added 155 new candidates, resulting in a sample of 957 candidates. In the next section, we classify the youth of 382 of those 957 candidates using new spectra that we have collected. Five additional candidates (2MASS J16232181–2424577, 2MASS J16250449–2509114, 2MASS J16260214–2718141, 2MASS J15562344–2541056, 2MASS J16212830–2529558) exhibit evidence of youth in previous spectroscopy (Martín et al. 1998; Tucker et al. 2015; Chinchilla et al. 2020). There remain 567 candidates that lack sufficient spectroscopic data to assess their youth, which are listed in Table 1 with their available spectral classifications, astrometry and photometry from *Gaia* DR2, and IR photometry. The central concentration of Upper Sco (Figure 5) contains ~ 200 of these candidates.

Esplin et al. (2018) presented 30 candidate disk-bearing members of Upper Sco that lacked spectroscopic confirmation of their youth, 26 of which satisfy the selection criteria described in this section. Three of the remaining candidates are rejected based on their astrometry from *Gaia* DR2 (AllWISE J162204.36–240814.5, AllWISE J155233.92–265112.5, AllWISE J155125.62–270743.4) and one candidate (2MASS J16214330–2345490) no longer satisfies one of the CMDs from Luhman et al. (2018) due to our new adjustments to the UKIDSS photometry.

Among the 567 candidates in Table 1, 28 are within $5''$ of known young stars, and thus are candidate companions. All of these candidates have parallaxes and proper motions from *Gaia* DR2 that support membership in Upper Sco. For each candidate, we include in Table 1 the separation and *Gaia* designation of the nearest known young star within $5''$. In addition, there are 17 pairs of candidates in Table 1 that have separations less than $5''$, which may also comprise binary systems.

Six of the candidates in Table 1 are bright enough that they should be easily detected by *Gaia* ($i < 15$ mag, $J < 13$ mag) but are absent from DR2. Forty-four candidates have *Gaia* counterparts but lack parallax measurements, 34 of which have $\text{RUWE} > 1.6$, indicating poor astrometric fits.

We estimated the completeness limits of the H and K photometry from UKIDSS to be 17.4 and 17.0 mag, respectively, based on the magnitudes at which the logarithm of the number of sources as a function of magnitudes departs from a linear slope and begins to turn over. When those limits are combined with the sequence of known members of Upper Sco in spectral type versus H and K (Luhman et al. 2018), they imply a completeness limit of $\sim L0$ ($\sim 0.01 M_{\odot}$) for our survey for candidate members.

As mentioned at the start of this section, the survey for candidate members of Upper Sco from Luhman et al. (2018) and in this work applies to an area outside of the boundary of Ophiuchus adopted by Esplin et al. (2018). Esplin & Luhman (2020) presents a catalog of candidate members of Upper Sco and Ophiuchus within

⁶ The errors in proper motion offsets include both the errors in the proper motions and the errors in the expected motions due to the parallax measurements.

that boundary.

3.2. Spectroscopy of Candidates

Luhman et al. (2018) and Esplin et al. (2018) obtained optical and IR spectra of several hundred candidate members of Upper Sco to measure their spectral types and check for signatures of youth that would support their membership. We have continued that work through spectroscopy of additional candidates. Our observations were performed with the 4 m Blanco telescope at the Cerro Tololo Inter-American Observatory (CTIO), the Magellan Baade telescope at Las Campanas Observatory, the NASA Infrared Telescope Facility (IRTF), the Bok Reflector at Steward Observatory, and the Gemini North and South telescopes. The instrument configurations are summarized in Table 2. We collected spectra of 430 objects, which are listed in Table 3 with the instrument and date of each observation. We also have made use of a publicly available spectrum of one additional candidate, 2MASS J16173081–2411411, that was taken at Gemini North through program GN-2018A-Q-115 (M. Liu). When selecting these targets, we gave highest priority to candidates within the central concentration in Upper Sco (Figure 5). One of the targets is a previously known member that was mistakenly observed with spectroscopy (*Gaia* 6049502122647926912). Most of the targets (401) satisfy our latest criteria for candidate members from the previous section. Among the remaining 29 targets, 21 were candidates from Luhman et al. (2018) that were observed before our selection criteria involving *Gaia* DR2 were finalized; one was observed because of IR excess emission and a previous classification that was uncertain (*Gaia* 6243223873758073728, Esplin et al. 2018); two were classified as galaxies by Luhman et al. (2018) and Esplin et al. (2018) based on emission lines and featureless continua in IR spectra, but *Gaia* DR2 data supported membership, so they were observed again in this work (*Gaia* 6242434969863194880 and 6243210920137332096); and five were observed because they are located within a few arcseconds of candidate members (*Gaia* 6045893074511675008, 6051816251024722176, 6049264044017673856, and 6045405136172296192 and 2MASS J16100274–2344400).

We reduced the SpeX data with the Spextool package (Cushing et al. 2004), which included correction of telluric absorption (Vacca et al. 2003). The spectra from the other instruments were reduced using routines within IRAF. We present examples of the reduced optical and IR spectra in Figures 7 and 8, respectively. The reduced spectra are provided in electronic files that accompany those figures. The optical spectra typically have signal-to-noise ratios (S/N’s) of ~ 50 at 7400–7500 Å. Most of the IR spectra exhibit S/N ~ 50 –100 in the *H* and *K* bands when binned to the lowest resolution among those data (~ 150).

We have analyzed our spectra with the same methods employed in our recent surveys for new members of Upper Sco (Esplin et al. 2018; Luhman et al. 2018). In brief, we examined the spectra for evidence that the targets are young enough to be members of Upper Sco (~ 10 Myr) based on Li absorption at 6707 Å and gravity-sensitive features like the Na doublet near 8190 Å and the near-IR H₂O absorption bands. We also measured spectral types

via comparison to standard spectra for field dwarfs (Kirkpatrick et al. 1991, 1997; Henry et al. 1994; Cushing et al. 2005; Rayner et al. 2009) and members of star-forming regions (Luhman et al. 1997; Luhman 1999; Luhman et al. 2017). Our measurements of spectral types, equivalent widths of Li, and assessments of youth are listed in Table 3. Most of the targets (376/431) exhibit evidence of youth. Comments on the classifications of individual sources are provided in the Appendix.

4. CLASSIFYING THE MEMBERSHIP OF YOUNG STARS TOWARD UPPER SCO

Luhman et al. (2018) compiled a catalog of 1631 stars that exhibited evidence of membership in Upper Sco and that are located outside of the boundary of Ophiuchus defined by Esplin et al. (2018). We have updated the analysis that produced that catalog to include the new young stars from this work, a few young stars toward Upper Sco from previous studies that were absent in Luhman et al. (2018), and constraints on membership provided by astrometry from *Gaia* DR2 (Section 2.2).

We have compiled all stars within the survey field considered by Luhman et al. (2018) (see Section 3.1) that exhibit evidence of youth from previous studies and this work. As done in that study, we include a few stars outside of that field that have been widely adopted as members of Upper Sco. Early-type stars lack spectroscopic signatures of youth, so we have considered all A and B stars that do not have parallax or proper motions that are highly discrepant ($> 2 \sigma$) from the membership criteria in Section 3.1. The resulting sample contains 2020 objects and is presented in Table 4. We have tabulated the available measurements of spectral types, our adopted types, our extinction estimates, proper motions and parallaxes from *Gaia* DR2, radial velocities from *Gaia* and previous studies, our calculations of *UVW* space velocities based on the astrometry from *Gaia* and the radial velocities, photometry from *Gaia* DR2, *JHK_s* photometry from various sources, our kinematic classifications of membership, and a flag indicating whether each object is adopted as a member of Upper Sco in this work. A similar catalog for young stars within the boundary of Ophiuchus is presented by Esplin & Luhman (2020). In the remainder of this section, we provide details concerning the data and membership classifications in Table 4.

4.1. Membership Classifications

For each star in Table 4 that has proper motion and parallax measurements from *Gaia* DR2, we have checked whether it overlaps at 1σ with the membership criteria in Section 3.1 for Upper Sco, Ophiuchus, or the remainder of Sco-Cen (V1062 Sco, UCL, LCC). If a parallax measurement is inconsistent at 1–2 σ but has an error of $> 10\%$, we ignore that measurement for this analysis. In addition, if either the parallax or proper motion differs by $> 1 \sigma$ from the criteria and the value of RUWE is greater than 1.6, that measurement is ignored. The same approach was taken in Section 3.1 when identifying candidate members. If the criteria for a given population are satisfied, a flag for that population is assigned to the star in Table 4: “O” for Ophiuchus, “U” for Upper Sco, and “S” for the remainder of Sco-Cen. The flag is upper case if the criteria for both proper motion and parallax are satisfied and it is lower case if the criterion for one

parameter is satisfied while the other parameter has been ignored. Since the criteria for the three populations overlap, some stars are consistent with multiple populations. We also assign a flag of “n” for stars that have *Gaia* data that are not consistent with any of the three populations.

We have adopted stars as members of Upper Sco if they have 1) flag = U, 2) flag = u and flag \neq S, or 3) flag is absent (i.e., the necessary *Gaia* data are not available). It is likely that a small minority of the stars in the third category (mostly late-type objects) are members of UCL/LCC given that kinematic members of UCL/LCC extend across Upper Sco on the sky (Figure 5). In Table 4, we indicate whether each star is adopted as a member of Upper Sco based on these criteria. We also have assigned membership in Upper Sco to a small number of stars that have flag \neq U/u, consisting of six stars for which parallaxes or proper motions changed significantly between DR1 and DR2 of *Gaia*, three objects that are only slightly beyond one of the kinematic thresholds for membership in Upper Sco, and three stars that are within a few arcseconds (i.e., likely companions) of kinematic members of Upper Sco. We have adopted 1761 of the 2020 stars in Table 4 as members of Upper Sco. We discuss the membership of a few individual stars in the Appendix.

4.2. Spectral Types and Extinctions

Two objects in Table 4 lack spectral classifications: *Gaia* 6242434969863194880 has strong IR excess emission and a featureless near-IR spectrum except for emission lines and ν Sco B has not been observed with spectroscopy. In addition, we do not list adopted spectral types for Antares, UGCS J161152.78–193847.3, and WISEA J161935.70–195043.0. The former is a red supergiant and the latter two sources have uncertain classifications (Cody et al. 2017; Esplin et al. 2018, Appendix). We have estimated extinctions for stars in Table 4 that have adopted types using (in order of preference) near-IR spectra, $J - H$, $J - K_s$, $H - K_s$, and $G_{BP} - G_{RP}$ relative to the typical intrinsic spectra and colors of young stars (Luhman et al. 2017, Appendix). For companions that lack these data, we adopt the extinction estimates of their primary stars. The reddenings are converted to extinction in K_s using relations from Indebetouw et al. (2005) and Schlafly et al. (2016) and $E(G_{BP} - G_{RP})/E(J - H) \approx 3$, where the latter is based on our sample of young stars toward Upper Sco. Although it has a spectral classification, we have not estimated an extinction for *Gaia* 6243210920137332096 due to the presence of strong near-IR excess emission.

4.3. Radial Velocities and UVW Velocities

In Table 4, we have included previous measurements of radial velocities that have errors less than 4 km s^{-1} , which are available for 293 stars. We omitted velocities with errors larger than that threshold because they would have little value in constraining the internal kinematics of Upper Sco given its velocity dispersion ($1\text{--}2 \text{ km s}^{-1}$, Wright & Mamajek 2018). We adopt errors of 0.4 km s^{-1} for velocities from Torres et al. (2006) for which errors were not reported, which is near the typical precision estimated in that study.

Among the 293 stars with radial velocities, 270 have *Gaia* measurements of proper motions and parallaxes

with errors of $\leq 10\%$. Four of the remaining 23 stars lack counterparts in *Gaia* DR2, all of which are bright enough for detection by *Gaia* (e.g., Antares). The other 19 stars have entries in DR2 and are sufficiently bright for precise parallaxes, but most of them have large values of RUWE, indicating poor astrometric fits. For 267 of the 270 stars with radial velocities and small relative errors in proper motion and parallax, we have used the radial velocities, proper motions, and parallactic distances (Bailer-Jones et al. 2018) to compute *UVW* space velocities (Johnson & Soderblom 1987), which are provided in Table 4. The errors for the space velocities were estimated through a Monte Carlo approach in which the realizations were generated with the python package *pyia* (Price-Whelan 2018) using the radial velocity errors and the covariance matrices of errors and correlation coefficients for the *Gaia* astrometry. Three of the 270 stars (USco CTIO 55, HD 148184, *Gaia* 6242801833086694528) were excluded from the calculations of *UVW* because their parallaxes are discrepant relative to members of Upper Sco and may be unreliable based on some combination of a large value of RUWE, an unusually large parallax error for a given magnitude, or a large change in parallax measurement between DR1 and DR2 of *Gaia*.

Among the 267 stars with *UVW* estimates, 209 are adopted as members of Upper Sco in Table 4. The median of the space velocities for those members is $U, V, W = -5.1, -16.0, -7.2 \text{ km s}^{-1}$, which is similar to the value derived by Wright & Mamajek (2018) for a smaller sample of members that had parallax and proper motion measurements from *Gaia* DR1. The standard deviations of the velocity components are $\sigma_{UVW} = 4.1, 1.4, 2.1 \text{ km s}^{-1}$. The latter two values are similar to the intrinsic velocity dispersions in V and W estimated by Wright & Mamajek (2018). Our standard deviation in U is larger than the dispersion U from that study because the radial velocity errors tend to be larger than the proper motion errors for this sample of stars, and the former contribute primarily to the errors in U .

5. PROPERTIES OF THE STELLAR POPULATION

5.1. Initial Mass Function

The IMF for Upper Sco has been previously estimated using samples of a few hundred members (Slesnick et al. 2008; Lodieu et al. 2011a; Lodieu 2013). The current census of members is much larger and more complete than those earlier samples, enabling a more accurate characterization of the IMF. For our analysis, we consider the adopted members from Table 4 that are within the central concentration of stars (Figure 5), which is where the completeness is greatest. We define the vertices of that field to be $(l, b) = (356.8^\circ, 25.2^\circ)$, $(347.4^\circ, 24.5^\circ)$, and $(356.8^\circ, 25.2^\circ)$. We exclude Antares and members with uncertain spectral classifications (Section 4.2) since we wish to use the distribution of spectral types as a proxy for the IMF, as done in our previous work (e.g., Luhman et al. 2016; Esplin & Luhman 2019). The resulting sample contains 1422 adopted members. The field in question also encompasses 204 candidate members from Table 1. Most of those candidates have not been observed with spectroscopy, so we have estimated their spectral types using their K_s photometry and the median relation between that band and spectral type for the known

member (i.e., the median of the sequence of members in K_s versus spectral type). For the small number of candidates that lack IR photometry (close companions resolved by *Gaia*), we have estimated spectral types with the median relation between G and spectral type. Most of the brighter candidates with photometry indicative of $\lesssim M6$ have parallax and proper motion measurements from *Gaia*, and thus are likely to be members.

In Figure 9, we present the distribution of spectral types for the adopted members in the central concentration of Upper Sco and the distribution that combines the adopted and candidate members. The addition of the candidates has little effect on the shape of the distribution at $< M9$. Regardless of whether the candidates are included, the distribution peaks at M5, which corresponds to masses of $\sim 0.15 M_\odot$ for the age of Upper Sco according to evolutionary models (Baraffe et al. 1998, 2015). The shape of the mass function at $\gtrsim L0$ ($\lesssim 0.01 M_\odot$) does depend significantly on the fraction of candidates that are members. Spectroscopy of those candidates will be necessary to better constrain the IMF in that mass range.

For comparison to Upper Sco, we have included in Figure 9 the spectral type distributions for extinction-limited samples of stars in Taurus (Esplin & Luhman 2019) and IC 348 (Luhman et al. 2016) and for a sample of members of the Orion Nebula Cluster (ONC) that was selected by Luhman (2018) with data from Da Rio et al. (2012) and Hillenbrand et al. (2013). The four regions have similar distributions from $\gtrsim K4$ ($\lesssim 1 M_\odot$) down to their completeness limits, most notably in terms of the shared peak at M5. At earlier types, the distributions in Taurus and IC 348 have large statistical errors because of the small numbers of stars, but the distributions in Upper Sco and the ONC are sufficiently populated that they exhibit a significant difference. The latter is likely a reflection of the evolution of the spectral types of the high-mass stars between the ages of the ONC and Upper Sco (~ 2 – 10 Myr, Hillenbrand 1997; Reggiani et al. 2011; Pecaut et al. 2012; Pecaut & Mamajek 2016).

5.2. Disk Fraction

Mid-IR photometry from *WISE* and the *Spitzer Space Telescope* (Fazio et al. 2004; Rieke et al. 2004; Werner et al. 2004)⁷ has been previously used to search for circumstellar disks in Upper Sco and estimate the fraction of members that harbor disks (Carpenter et al. 2006, 2009; Chen et al. 2011; Luhman & Mamajek 2012; Riaz et al. 2012; Dawson et al. 2013; Rizzuto et al. 2012, 2015; Pecaut & Mamajek 2016; Esplin et al. 2018). As with the IMF, we can measure the disk fraction in Upper Sco with a catalog of members that is larger and more complete than the samples that were available in previous disk studies.

Luhman & Mamajek (2012) and Esplin et al. (2018) used photometry in three bands from *WISE* ($W2$, $W3$, $W4$) and three bands from *Spitzer* ($[4.5]$, $[8.0]$, $[24]$) to identify excess emission from disks among members of Upper Sco and to classify the evolutionary stages of the

detected disks. The available *Spitzer* images encompass only a subset of the members of Upper Sco, but they offer better sensitivity than the all-sky data from *WISE*. We have updated the classifications from Luhman & Mamajek (2012) and Esplin et al. (2018) using our latest extinction estimates and adopted spectral types (Table 4) and our new estimates for the typical intrinsic colors of young stellar photospheres (Appendix). We also have checked for mid-IR excesses among the new stars that now appear in our membership catalog. For our adopted members, we present in Table 5 a compilation of photometry from *WISE* and *Spitzer*, indicators of excess emission in the six considered bands, and disk classifications. Data are unavailable in any of those bands for 49 objects, which are unresolved from brighter stars or below the detection limits.

For their sample of Upper Sco members with mid-IR data, Luhman & Mamajek (2012) calculated the fraction with excess emission as a function of spectral type in $[4.5]/W2$, $[8.0]$, $W3$, and $[24]/W4$. The excess classifications in $[4.5]/W2$ and $[24]/W4$ were combined since the filters in each pair have similar effective wavelengths ($4.5/4.6$ and $23.7/22 \mu\text{m}$). We have repeated that analysis using our compilation of mid-IR data in Table 5. Since some of the stars in our catalog for Upper Sco were originally identified as candidate members via signatures of disks (Esplin et al. 2018), the current census could be biased in favor of disk-bearing members, which would mean that the excess fractions computed from that sample are not representative of the stellar population. To minimize a bias of that kind, we have included in our excess fractions the 313 candidate members from Table 1 that have parallaxes and proper motions from *Gaia* and photometry from *WISE* or *Spitzer*, which encompasses most of the candidates that are likely to be earlier than $\sim M7$. That sample should have little contamination from non-members based on our spectroscopy of *Gaia*-selected candidates (Section 3.2). There remain 65 *Gaia* candidates that were unresolved from brighter stars in the mid-IR images. Given that Esplin et al. (2018) already obtained spectra of most candidates for disk-bearing members from *WISE*, only a small number (13) of the 313 remaining candidates with *Gaia* and *WISE* data exhibit possible excess emission. Most of the excesses are small enough that they are indicative of debris or evolved transitional disks (Espaillat et al. 2012). We have not attempted to include in the excess fractions the candidates that are too faint for *Gaia* parallaxes because their membership is less certain. At the spectral types expected for those faint candidates ($\gtrsim M9$), only a few members have been identified based on disk signatures (Esplin et al. 2018), so the sample of known members should not be biased in terms of disks, and hence their disk fraction should be representative of the stellar population.

The images in $W2$, $[4.5]$, and $[8.0]$ detected nearly all adopted members of Upper Sco that were encompassed by them and that were not blended with brighter stars. However, some late-type members were too faint for detection in $W3$, $W4$, and $[24]$, particularly those that lack disks. As a result, excess fractions in those bands would be biased in favor of disks at the latest spectral types. Therefore, as done in Luhman & Mamajek (2012), we have computed the excess fraction in each of those bands

⁷ *WISE* observed in bands centered at 3.5, 4.5, 12, and 22 μm , which are denoted as $W1$, $W2$, $W3$, and $W4$, respectively. *Spitzer* obtained images primarily in bands at 3.6, 4.5, 5.8, 8.0 and 24 μm , which are denoted as $[3.6]$, $[4.5]$, $[5.8]$, $[8.0]$, and $[24]$, respectively.

only for the range of spectral types in which most members and candidates are detected. The $W4/[24]$ fraction is based on data from [24] for $\leq M4$ when available and otherwise uses $W4$ for $\leq M0$. There are ~ 70 stars that are earlier than $M4$ and have useful non-detections⁸ in [24] or are earlier than $M0$ and have non-detections in $W4$. All of these non-detections are sufficient to indicate that any excesses must be quite small ($\lesssim 0.5$ mag), corresponding to debris or evolved transitional disks. We assume that these stars lack excesses for the calculation of the excess fraction in $W4/[24]$. The $W3$ excess fraction is computed for stars earlier than $M4$, among which a dozen have useful non-detections. As with $W4$ and [24], those non-detections demonstrate that little excess emission is present, so we assume that excesses are absent for the $W3$ fractions.

We present the excess fractions as a function of spectral type for [4.5]/ $W2$, [8.0], $W3$, and [24]/ $W4$ in Table 6 and Figure 10. As done in Luhman & Mamajek (2012), for each band and spectral type range we have computed one excess fraction for three classes of primordial disks (full, evolved, transitional) and one fraction for evolved transitional and debris disks. The latter two classes contain primordial and second-generation dust, respectively, but they are grouped together because they are indistinguishable in the available mid-IR data. The excess fractions are generally similar to those from Carpenter et al. (2006) and Luhman & Mamajek (2012) for smaller samples of members. For the primordial disks, the excess fractions decrease slightly from longer to shorter wavelengths at a given spectral type, which is a reflection of clearing of inner disks for the transitional and evolved classes, and it increases with later spectral types for a given band. Meanwhile, the excess fraction for debris and evolved transitional disks is higher for longer wavelengths and earlier types.

In addition to the excess fractions for specific bands, we have estimated the primordial disk fraction as a function of spectral type based on the fraction of stars that exhibit excess emission in any band and that are classified as full, evolved, or transitional. The results are presented in Table 7 and Figure 11. As done in our previous studies (Luhman et al. 2010, 2016; Esplin & Luhman 2019), we have derived the fractions for $< K6$, $K6$ – $M3.5$, $M3.75$ – $M5.75$, $M6$ – $M8$, and $M8$ – $M9.75$, which approximate logarithmic mass intervals for stars with ages of $\lesssim 10$ Myr (Baraffe et al. 1998, 2015). These calculations omit stars that lack the mid-IR data needed for assessing the presence of excesses. As with the excess fractions, the disk fractions increase with later spectral types, although the variation of disk fraction is more subtle since the highest mass bin encompasses a wide range of types.

5.3. Stellar Ages

Previous studies have estimated the ages of the three subgroups in Sco-Cen using several diagnostics, most notably the main-sequence turnoffs and the empirical isochrones formed by low-mass members in the Hertzsprung-Russell (H-R) diagram (Preibisch & Mamajek 2008; Pecaute et al. 2012; Song et al. 2012). Based on

the methods applied to the more massive stars ($\gtrsim 1 M_{\odot}$), Pecaute & Mamajek (2016) adopted ages of ~ 10 , 16, and 15 Myr for Upper Sco, UCL, and LCC, respectively. At lower masses, ages have been derived primarily in Upper Sco since it has been searched more extensively for low-mass members than the other subgroups. The ages inferred for the low-mass stars in Upper Sco from the H-R diagram have been significantly younger than the ages found at higher masses (~ 5 Myr, de Geus et al. 1989; Preibisch et al. 2002; Herczeg & Hillenbrand 2015). However, evolutionary models that account for the inhibition of convection by magnetic fields have largely removed this discrepancy by producing older isochronal ages for the low-mass stars (Feiden 2016; MacDonald & Mullan 2017; Asensio-Torres et al. 2019). The magnetic models also have reproduced the measured radii of low-mass eclipsing binaries in Upper Sco for those older ages (Kraus et al. 2015; David et al. 2016a, 2019).

Gaia has provided high-precision parallaxes and photometry for a large number of low-mass stars in Sco-Cen, which we can use to measure accurate empirical isochrones in CMDs for the subgroups and estimate the relative ages of the subgroups and other nearby associations. To construct these isochrones, we consider a range of colors in which 1) precise parallaxes are available for Sco-Cen ($\pi/\sigma > 50$) and 2) the shapes of theoretical isochrones remain mostly unchanged for ages of ~ 1 – 30 Myr (e.g., stars with different masses experience similar evolution in their luminosities), which corresponds to $G_{BP} - G_{RP} = 1.4$ – 2.8 mag (~ 0.2 – $1 M_{\odot}$, $K5$ – $M4$). Herczeg & Hillenbrand (2015) derived empirical isochrones for young clusters and associations within a similar range of spectral types.

In Figure 12, we show $M_{G_{RP}}$ versus $G_{BP} - G_{RP}$ for four samples of stars in Sco-Cen that are between $G_{BP} - G_{RP} = 1.4$ – 2.8 mag: 1) members of Upper Sco from Table 4 that are within the central concentration employed for our IMF measurement (Section 5.1) and have $A_V < 1$ mag, 2) stars that are within the 2σ ellipses for the V1062 Sco cluster from Figure 4 and are within 2° from V1062 Sco, 3) stars that are within the ellipses for UCL/LCC from Figure 4 and are within the boundary of UCL from Figure 5, and 4) stars that are within the ellipses for UCL/LCC and are within the boundary of LCC. Since stars with accretion disks can exhibit excess emission in short-wavelength bands like G_{BP} , we have excluded stars that have evidence of disks in their mid-IR photometry from *Spitzer* and *WISE*. A typical reddening vector for the intrinsic colors and levels of extinction of the Upper Sco sample is shown in Figure 12. Reddening and the sequence in Upper Sco have similar slopes, but they differ enough for reddening to have a noticeable effect on the vertical position of the sequence, so we have dereddened the photometry for Upper Sco using the extinctions from Table 4 and have considered only members with $A_V < 1$ mag, as mentioned earlier. Most known members of UCL and LCC have $A_V < 0.5$ mag (Pecaute & Mamajek 2016), so we have not dereddened the data for the other Sco-Cen samples in Figure 12.

For comparison to the Sco-Cen samples, we have included in Figure 12 members of 32 Ori and β Pic because they are two of the youngest nearby associations that have ages estimated with the lithium depletion boundary (~ 21 – 24 Myr, Binks & Jeffries 2014, 2016; Bell et

⁸ We are referring to non-detections that provide useful flux limits, namely those that are not due to bright extended emission or blending with other stars.

al. 2015, 2017; Shkolnik et al. 2017), which is one of the most reliable age diagnostics for stellar populations with ages between 20–200 Myr (Soderblom et al. 2014). We have adopted the members of 32 Ori from Bell et al. (2017) and the members of β Pic from Bell et al. (2015) and Gagné & Faherty (2018). We have omitted a few of those stars that are discrepant in terms of their kinematics and positions in CMDs based on *Gaia* data. Previous studies have found that the TW Hya and η Cha associations are roughly coeval with Upper Sco (e.g., Herczeg & Hillenbrand 2015), so we have also plotted their diskless members in the CMD for Upper Sco to enable a direct comparison. The sequences for TW Hya and η Cha do agree well with that of Upper Sco, confirming that they have similar ages.

Each of the samples in Figure 12 is shown with a fit to the median of the combined sequence for UCL and LCC, which facilitates visual comparison of the sequences. To compare the sequences quantitatively, we begin by computing the offset of each star in $M_{G_{\text{RP}}}$ from the fit to UCL/LCC. We then computed the difference between the median offset for a given population and the median offset for the β Pic sequence. The error in that difference was characterized using the median absolute deviation (MAD) for the distribution of differences produced by bootstrapping. The resulting differences in $M_{G_{\text{RP}}}$ relative to β Pic are 0.49 ± 0.04 (Upper Sco), 0.15 ± 0.06 (V1062 Sco), 0.09 ± 0.02 (UCL), 0.14 ± 0.02 (LCC), and 0.12 ± 0.06 mag (32 Ori). Since UCL and LCC appear to be coeval, we also computed the difference between their combined sequence and β Pic, which is 0.10 ± 0.02 mag.

We have converted the differences in $M_{G_{\text{RP}}}$ for Upper Sco and UCL/LCC to differential ages using the luminosity evolution predicted by standard non-magnetic models (Baraffe et al. 2015; Choi et al. 2016; Dotter 2016) and new versions of the magnetic models from Feiden (2016) provided by G. Feiden (private communication). The non-magnetic and magnetic models predict similar changes in luminosity with age between 10 and 25 Myr. Relative to β Pic, Upper Sco is younger by 0.30 ± 0.025 dex (a factor of two) and UCL/LCC is younger by 0.060 ± 0.024 dex according to both the non-magnetic and magnetic models. Based on the lithium depletion boundary in β Pic, Binks & Jeffries (2016) estimated ages of 21 ± 4 and 24 ± 4 Myr with non-magnetic and magnetic models, respectively. For those ages, our differential measurements imply ages of 10.5 and 12 Myr for Upper Sco and ages of 18 and 21 Myr for UCL/LCC. The latter three values are slightly older than most of the ages reported in recent studies of Sco-Cen (Pecaut et al. 2012; Pecaut & Mamajek 2016). Meanwhile, our analysis indicates that V1062 Sco and 32 Ori have similar ages as UCL/LCC, although their differential ages have larger errors due to the smaller samples. Based on lithium depletion and isochrones, age estimates for 32 Ori and β Pic have agreed to within ~ 1 Myr and have had errors of ± 4 Myr (Mamajek & Bell 2014; Bell et al. 2017). However, the sequences in Figure 12 suggest that 32 Ori is younger than β Pic by ~ 3 Myr.

Donaldson et al. (2017) measured parallaxes for 48 K/M stars that were adopted as members of Upper Sco, 47 of which are also in our catalog of members. The parallaxes were used to place the stars on the H-R diagram and ages were estimated from the evolutionary

models of Baraffe et al. (2015). Donaldson et al. (2017) found that the diskless and disk-bearing stars exhibited median ages of 3.4 and 6.5 Myr, respectively, which corresponds to a difference of ~ 0.45 mag in luminosity. We have performed a similar age comparison using the new parallaxes and membership classifications that are now available. We consider members of Upper Sco from Table 4 that have $\pi/\sigma > 50$, $A_V < 1$ mag, $\text{RUWE} < 1.6$, and spectral types of K5–M4, which corresponds to a sample of 334 stars, 45 of which have evidence of disks. Since G_{BP} can be contaminated by accretion-related emission, we placed the stars in an H-R diagram that uses spectral type instead of $G_{\text{BP}} - G_{\text{RP}}$. As in our earlier analysis, we used extinction-corrected $M_{G_{\text{RP}}}$ for the vertical axis of the H-R diagram. We derived a fit to the median of the sequence for our sample and computed the $M_{G_{\text{RP}}}$ offset of each star from the median. The median offsets of the disk-bearing and diskless samples differ by only 0.05 mag and both samples have MADs of 0.45 mag. Thus, we find no significant difference in the ages of diskless and disk-bearing stars in Upper Sco.

6. CONCLUSIONS

We have refined the census of stars and brown dwarfs in the Upper Sco subgroup within the Sco-Cen OB association using high-precision parallaxes and proper motions from *Gaia* DR2 and optical and IR spectroscopy of candidate members. Using the resulting catalog of adopted members, we have examined the IMF, disk fraction, and median age in Upper Sco. Our results are summarized as follows:

1. We have used a CMD constructed with data from *Gaia* DR2 to identify candidate young stars within the boundary of Sco-Cen from de Zeeuw et al. (1999). We fit the kinematics of these stars with a Gaussian mixture model that contains three components for Sco-Cen, corresponding to Upper Sco/Ophiuchus/Lupus, the V1062 Sco cluster, and UCL/LCC. We have used the stars classified as likely members of Sco-Cen within the central concentration of the Upper Sco association to define kinematic criteria for membership within that population. The selection of candidate members of Upper Sco from Luhman et al. (2018) has been updated to include the application of those kinematic criteria to data from *Gaia* DR2. Our survey for candidates should be complete down to spectral types of $\sim L0$ ($\sim 0.01 M_{\odot}$) for the areas observed by UKIDSS, which corresponds to most of Upper Sco.
2. We have analyzed optical and IR spectra of 431 objects toward Upper Sco to measure their spectral types and check for signatures of youth that would support their membership, 376 of which are classified as young. Most of the latter have spectral types of late K through early L (~ 0.01 – $1 M_{\odot}$), including 42 that are M8 or later ($\lesssim 0.04 M_{\odot}$).
3. We have compiled 2020 objects toward Upper Sco that exhibit evidence of youth in previous studies and this work. Their membership in Upper Sco has been assessed using available proper motions and

parallaxes, most notably from *Gaia* DR2. Based on that analysis, we have adopted 1761 objects as members of Upper Sco. There remain 567 candidates from our survey that lack the necessary spectroscopy for confirming youth, 378 of which have accurate *Gaia* astrometry and hence are probable members. Thus, Upper Sco likely contains at least ~ 2100 members.

4. We have characterized the IMF in Upper Sco in terms of the distribution spectral types for the central concentration of the association. The distribution is similar to those in other star-forming regions like IC 348, Taurus, and the ONC, all of which peak near M5 ($\sim 0.15 M_{\odot}$).
5. Luhman & Mamajek (2012) and Esplin et al. (2018) compiled mid-IR photometry from *WISE* and *Spitzer* for previous samples of Upper Sco members and used those data to identify excess emission from disks and to classify the detected disks. Luhman & Mamajek (2012) also computed the fraction of members exhibiting excesses as a function of band and spectral type. We have presented an updated compilation of mid-IR photometry and disk classifications for our adopted members. The new excess fractions are qualitatively similar to those from Luhman & Mamajek (2012), reproducing a trend originally discovered by Carpenter et al. (2006) in which the excess fractions for primordial disks increase with later spectral types. The fraction of members with disks ranges from $\lesssim 10\%$ for $> 1 M_{\odot}$ to $\sim 22\%$ for $0.01\text{--}0.3 M_{\odot}$.
6. We have estimated the relative ages of Upper Sco, other populations in Sco-Cen, and the 32 Ori and β Pic associations using their sequences of low-mass stars in $M_{G_{\text{RP}}}$ versus $G_{\text{BP}} - G_{\text{RP}}$. According to non-magnetic/magnetic evolutionary models, the offsets in $M_{G_{\text{RP}}}$ among the sequences indicate that Upper Sco and UCL/LCC are younger than β Pic by 0.30 and 0.060 dex, respectively. Binks & Jeffries (2016) estimated ages of $21/24 \pm 4$ Myr for the β Pic association from the lithium depleting boundary using non-magnetic/magnetic models, which would imply ages of 10.5/12 Myr for Upper Sco and 18/21 Myr for UCL and LCC. Although β Pic and 32 Ori have been previously found to have ages that agree to within ~ 1 Myr (each with errors of ± 4 Myr), their sequences of low-mass stars indicate that 32 Ori is younger by ~ 3 Myr.

K.L. acknowledges support from NASA grant 80NSSC18K0444 for portions of this work. We thank Eric Feigelson for advice regarding statistical methods Gregory Feiden for providing his evolutionary models, and Eric Mamajek for comments on the manuscript. The IRTF is operated by the University of Hawaii under contract NNH14CK55B with NASA. The data at CTIO were obtained through program 2018A-0098 and 2019A-0127 at the National Optical Astronomy Observatory (NOAO). CTIO and NOAO are operated by the Association of Universities for Research in Astronomy under

a cooperative agreement with the NSF. The Gemini data were obtained through programs GN-2018A-Q-115, GN-2018A-Q-218 (NOAO 2018A-0066), GN-2019A-Q-317 (2019A-0086), GS-2019A-Q-125 (2019A-0053), and GN-2020A-Q-218 (2020A-0066). Gemini Observatory is operated by AURA under a cooperative agreement with the NSF on behalf of the Gemini partnership: the NSF (United States), the NRC (Canada), CONICYT (Chile), the ARC (Australia), Ministério da Ciência, Tecnologia e Inovação (Brazil) and Ministerio de Ciencia, Tecnología e Innovación Productiva (Argentina). *WISE* is a joint project of the University of California, Los Angeles, and the JPL/Caltech, funded by NASA. 2MASS is a joint project of the University of Massachusetts and IPAC at Caltech, funded by NASA and the NSF. This work used data from the NASA/IPAC Infrared Science Archive, operated by JPL under contract with NASA, and the SIMBAD database, operated at CDS, Strasbourg, France. This work has made use of data from the European Space Agency (ESA) mission *Gaia* (<https://www.cosmos.esa.int/gaia>), processed by the *Gaia* Data Processing and Analysis Consortium (DPAC, <https://www.cosmos.esa.int/web/gaia/dpac/consortium>). Funding for the DPAC has been provided by national institutions, in particular the institutions participating in the *Gaia* Multilateral Agreement. Funding for the Sloan Digital Sky Survey IV has been provided by the Alfred P. Sloan Foundation, the U.S. Department of Energy Office of Science, and the Participating Institutions. SDSS-IV acknowledges support and resources from the Center for High-Performance Computing at the University of Utah. The SDSS web site is www.sdss.org. SDSS-IV is managed by the Astrophysical Research Consortium for the Participating Institutions of the SDSS Collaboration including the Brazilian Participation Group, the Carnegie Institution for Science, Carnegie Mellon University, the Chilean Participation Group, the French Participation Group, Harvard-Smithsonian Center for Astrophysics, Instituto de Astrofísica de Canarias, The Johns Hopkins University, Kavli Institute for the Physics and Mathematics of the Universe (IPMU) / University of Tokyo, the Korean Participation Group, Lawrence Berkeley National Laboratory, Leibniz Institut für Astrophysik Potsdam (AIP), Max-Planck-Institut für Astronomie (MPIA Heidelberg), Max-Planck-Institut für Astrophysik (MPA Garching), Max-Planck-Institut für Extraterrestrische Physik (MPE), National Astronomical Observatories of China, New Mexico State University, New York University, University of Notre Dame, Observatório Nacional / MCTI, The Ohio State University, Pennsylvania State University, Shanghai Astronomical Observatory, United Kingdom Participation Group, Universidad Nacional Autónoma de México, University of Arizona, University of Colorado Boulder, University of Oxford, University of Portsmouth, University of Utah, University of Virginia, University of Washington, University of Wisconsin, Vanderbilt University, and Yale University. The Center for Exoplanets and Habitable Worlds is supported by the Pennsylvania State University, the Eberly College of Science, and the Pennsylvania Space Grant Consortium.

APPENDIX

COMMENTS ON INDIVIDUAL SOURCES

Gaia 6045893078810161152 (M0.25) and 6045893074511675008 (M3.75) comprise a 3''/8 pair. Their parallaxes and proper motions differ by $> 1 \sigma$, but they are roughly similar, which would suggest that they are companions given their small separation. The first component has a large enough value of RUWE (2.6) to suggest a poor astrometric fit, so it may not be surprising that their kinematics do not agree more closely. However, Li absorption is strong in *Gaia* 6045893078810161152 (0.54 Å) and absent in *Gaia* 6045893074511675008 (< 0.1 Å), indicating that they are not coeval and thus are not companions, or that the latter has experienced an unusual degree of Li depletion. For the purposes of this work, we classify *Gaia* 6045893074511675008 as a nonmember based on the old age implied by its lack of Li absorption (> 30 Myr).

The near-IR spectrum of UGCS J161152.78–193847.3 exhibits strong steam absorption that indicates a spectral type of late M or L and a triangular *H*-band continuum that indicates a young age (Lucas et al. 2001). However, the (very red) slope of the spectrum does not agree well with standard spectra for young M/L objects (Luhman et al. 2017), even when including reddening as a free parameter. Stars that are observed primarily in scattered light (e.g., edge-on disks) can have anomalous spectral slopes at near-IR wavelengths (Luhman et al. 2007). UGCS J161152.78–193847.3 is one of the reddest objects in our catalog of adopted members of Upper Sco in its IR colors ($J - K_s = 2.63$ mag, $W1 - W2 = 1.07$ mag). It has an uncertain detection in *W3* and no detection in *W4*. These constraints on its IR colors fall within the ranges of colors observed for young stars with edge-on disks in Taurus (Esplin et al. 2014). High-resolution imaging and additional long-wavelength photometry would be useful for further testing the presence of an edge-on disk around UGCS J161152.78–193847.3.

GSC 06214-00210 is a K7 star that has been previously classified as a member of Upper Sco (Preibisch et al. 1998). It harbors a substellar companion at a separation of 2''/2, which has a mass of $\sim 14 M_{\text{Jup}}$ according to evolutionary models assuming an age of 5 Myr for Upper Sco (Bowler et al. 2011; Ireland et al. 2011). However, the *Gaia* proper motion offset and parallax of GSC 06214-00210 ($\Delta\mu_{\alpha,\delta} \sim -6.3, -0.6$ mas yr $^{-1}$, $\pi = 9.188$ mas) are inconsistent with the criteria for membership in Upper Sco in Figure 6, and instead indicate membership in UCL/LCC. Applying the older age of UCL/LCC to the secondary would result in a higher estimate of its mass.

EPIC 203710387 is an eclipsing binary that is projected against Upper Sco. Its components are fainter and smaller in radius than expected for members of Upper Sco, indicating an older age (David et al. 2019). The system's kinematics in Figure 6 are consistent with membership in either Upper Sco or UCL/LCC. Given that the kinematic members of UCL/LCC extend across Upper Sco (Fig. 6), the data from David et al. (2019) could be explained by membership in UCL/LCC.

EXTINCTION COEFFICIENTS IN *GAIA* BANDS

Gaia Collaboration et al. (2018a) derived formulae for extinction coefficients in G , G_{BP} , and G_{RP} , which were defined as ratios of the extinctions in those bands relative to the extinction at 5500 Å ($k_\lambda = A_\lambda/A_{5500}$). For broad filters like those from *Gaia* (Evans et al. 2018), extinction coefficients depend significantly on the distribution of flux across a filter, which is determined by both the extinction and intrinsic spectrum of an object. *Gaia* Collaboration et al. (2018a) estimated these dependencies by applying a range of extinctions ($A_{5500} = 0.01\text{--}5$ mag) to spectra over a range of effective temperatures (3500–10,000 K, $G_{\text{BP}} - G_{\text{RP}} \sim 0\text{--}2.2$ mag), adopting the extinction law from Fitzpatrick & Massa (2007) for $A_{5500} = 3.1E(B - V)$ and model spectra from Castelli & Kurucz (2004). For each *Gaia* band, the resulting extinction coefficients were fitted by polynomial functions containing A_{5500} and the intrinsic value of $G_{\text{BP}} - G_{\text{RP}}$.

Gaia is capable of detecting members of nearby star-forming regions with intrinsic colors and extinctions beyond the limits considered in the simulation of extinction coefficients by *Gaia* Collaboration et al. (2018a). For instance, *Gaia* DR2 provides detections in both G_{BP} and G_{RP} for members of Upper Sco with spectral types as late as \sim M7, which have intrinsic colors of $G_{\text{BP}} - G_{\text{RP}} \sim 4.3$ mag. Therefore, we have derived new formulae for the extinction coefficients in the *Gaia* bands that are applicable to wider ranges of extinctions and intrinsic colors. For this analysis, we have adopted the profiles for the *Gaia* filters from Maíz Apellániz & Weiler (2018), the extinction curve from Schlafly et al. (2016) for $x = 0$ ($R_V = A_V/E(B - V) \approx 3.3$), model spectra for 4000–10,000 K and $\log g = 4$ from Castelli & Kurucz (2004), and model spectra for 2600–4000 K and $\log g = 5$ from Baraffe et al. (2015). A lower limit of 2600 K was selected because it corresponds roughly to our desired limit of $G_{\text{BP}} - G_{\text{RP}} \sim 4.3$ mag. Like *Gaia* Collaboration et al. (2018a), we have fitted the simulated extinction coefficients with polynomials containing A_{5500} and intrinsic $G_{\text{BP}} - G_{\text{RP}}$. Since extinction is more commonly measured in a band rather than at a single wavelength, we also have fitted the coefficients as a function of A_V and $G_{\text{BP}} - G_{\text{RP}}$ where the V filter profile is taken from Mann & von Braun (2015). Our adopted formulae for the extinction coefficients are presented in Table 8, which apply to $A_{5500} \leq 20$ mag and $A_V \leq 20$ mag. The residuals for these fits are $\lesssim 1\%$, $\lesssim 2\%$, and $\lesssim 0.5\%$ for G , G_{BP} , and G_{RP} , respectively.

The validity of our simulated extinctions can be tested with the observed colors of reddened stars. We begin by defining a sample of red clump stars that are subject to varying amounts of extinction in the galactic plane using spectroscopic data that were obtained through the Apache Point Observatory Galactic Evolution Experiment (APOGEE, Majewski et al. 2017) and that are available in data release 15 of the Sloan Digital Sky Survey (Aguado et al. 2019). We have selected APOGEE targets that have 2MASS and *Gaia* DR2 counterparts and that exhibit $S/N > 50$, $K_s < 14$ mag, $-0.5 \leq [M/H] \leq 0$, $4800 \text{ K} \leq T_{\text{eff}} \leq 5000 \text{ K}$, and $2.35 \leq \log g \leq 2.55$. The latter three criteria were designed to encompass a large number of red clump stars while being narrow enough that the spread in intrinsic colors should be small. We also omit *Gaia* photometry that is fainter than a magnitude of 20 and 2MASS photometry with errors greater than 0.05 mag. In the left column of Figure 13, we plot color excesses in the *Gaia* bands relative to K_s versus excesses in $J - H$ for our sample of red clump stars. We have computed the excesses by subtracting intrinsic colors such that the blue end of each sequence of excesses is aligned with the origin, which consist of $G - K_s = 1.95$ mag, $G_{\text{BP}} - K_s = 2.45$ mag, $G_{\text{RP}} - K_s = 1.4$ mag, and $J - H = 0.52$ mag. For comparison, we plot our simulated excesses for $x = 0$ ($R_V \approx 3.3$) and a model spectrum with $T_{\text{eff}} = 5000 \text{ K}$ and $\log g = 2.5$. The simulated reddening vector agrees well with the slope of the observed color excesses. Such agreement is expected given that the adopted extinction curve from Schlafly et al. (2016) was measured with APOGEE targets in the galactic plane. To check whether that extinction curve is applicable to Upper Sco and Ophiuchus, we include in Figure 13 the color excesses for our compilation of young stars in those regions that lack excess emission from disks at $< 5 \mu\text{m}$. Since the reddening vectors depend on intrinsic stellar colors, we consider only two narrow ranges of spectral types, M0–M4 and M4–M6, that encompass a large number of stars, particularly ones at higher extinctions. We plot with those data our simulated reddening vectors for stars with the intrinsic colors of young M2 and M5 stars ($G_{\text{BP}} - G_{\text{RP}} \approx 2$ and 3 mag) and for $x = 0$ and $x = 2$ ($R_V \approx 3.3$ and 5). For each of the *Gaia* bands, the observed color excesses roughly follow the predicted vector for $x = 0$ at low extinctions, but diverge from it at $E(J - H) \gtrsim 0.5$ mag ($A_V \gtrsim 5$ mag). All of the latter stars are in the Ophiuchus clouds. The discrepancy is reduced to varying degrees among the bands with $x = 0.2$, which is qualitatively consistent with the previous measurements of unusually high values of R_V in Ophiuchus (Chini 1981; Chapman et al. 2009).

We have also examined the dependence of the extinction coefficient in the 2MASS K_s band ($k_K = A_K/A_V$) on A_V and effective temperature assuming the extinction curve from Schlafly et al. (2016). The simulated values of k_K for most temperatures range from 0.090–0.093 at $A_V \sim 0$ mag and from 0.10–0.105 at $A_V \sim 20$ mag. The middle of this sequence of coefficients can be fit by the following formula: $k_K = 0.0916 + 0.00036A_V + 0.0000089A_V^2$. The residuals from that fit exceed 2% only for highly reddened cool stars ($A_V > 10$ mag, $< 3500 \text{ K}$).

INTRINSIC COLORS OF YOUNG STARS AND BROWN DWARFS

By comparing the observed colors of a young star to the intrinsic photospheric colors expected for its spectral type, one can estimate the extinction along the line-of-sight to the star or the excess emission from circumstellar material. In analysis of that kind, the typical colors of main sequence stars are often adopted for the photospheric colors (Kenyon & Hartmann 1995), but some studies have estimated the intrinsic colors of young stars using members of nearby associations and star-forming regions (Luhman et al. 2010; Pecaut & Mamajek 2013, references therein). Given the recent availability of photometry from *Gaia* and the continued improvement in membership samples of nearby young populations, we have derived intrinsic colors of young stars in the *Gaia* bands and updated our estimates of colors in

other widely-used bands from 2MASS, *WISE*, and *Spitzer*. We have performed our analysis using known members of populations that have ages of $\lesssim 20$ Myr and distances of $\lesssim 150$ pc, consisting of Upper Sco (Section 4), Taurus (Esplin & Luhman 2019, references therein), and Chamaeleon I (Esplin et al. 2017, references therein) and the associations containing TW Hya (Webb et al. 1999; Sterzik et al. 1999; Gizis 2002; Zuckerman & Song 2004; Scholz et al. 2005; Looper et al. 2007, 2010a,b; Shkolnik et al. 2011; Kellogg et al. 2015; Schneider et al. 2012, 2016; Gagné et al. 2014, 2017), η Cha (Mamajek et al. 1999; Luhman & Steeghs 2004; Lyo et al. 2004), β Pic (Zuckerman et al. 2001; Schlieder et al. 2010, 2012; Shkolnik et al. 2017), and 32 Ori (Mamajek 2007; Bell et al. 2017).

We have adopted photometry for our sample from the 2MASS Point Source Catalog (JHK_s), the AllWISE Source Catalog ($W1$ – $W4$), *Gaia* DR2 (G , G_{BP} , G_{RP}), and the available observations with *Spitzer* (Luhman et al. 2010; Shvonski et al. 2016; Esplin et al. 2017, 2018; Esplin & Luhman 2019, references therein). We also make use of deeper near-IR data that are available from UKIDSS, VISTA VHS, and dedicated imaging (e.g., Esplin et al. 2017; Esplin & Luhman 2019). As done in Section 3.1, the data from UKIDSS and VHS have been adjusted so that they are calibrated to 2MASS for late-type objects.

Stars in our sample that are within the Local Bubble ($\lesssim 100$ pc) should have very little extinction ($A_V < 0.2$ mag, Reis et al. 2011), so their intrinsic colors should be reflected in their photometry as long as circumstellar disks are absent, which can produce color excesses. At a given spectral type, the bluest stars in the more distant populations like Upper Sco and Taurus have similar colors as the stars within the Local Bubble, indicating that the former also have little extinction and thus can provide constraints on the intrinsic colors. When estimating intrinsic colors as a function of spectral type from these data, we have given preference to stars that have the youngest ages (in case the colors vary with age) and no evidence of circumstellar disks. Thus, we have used the data from the β Pic and 32 Ori groups (24 Myr, Bell et al. 2017) only when insufficient data from younger regions are available for a given color and range of spectral types.

We have not estimated colors involving G_{BP} , $W3$, $W4$, and $[24]$ for some of the latest spectral types because too few objects are well-detected in those bands. We have not attempted to derive any intrinsic colors later than L0 given the large uncertainties in spectral types in that range (Luhman et al. 2017). Colors relative to some bands were not derived for $\leq B7$ due to the small number of observations ($[3.6]$, $[5.8]$) or saturation ($W1$). When comparing the $[4.5]$ and $W2$ data for our sample, we find no systematic differences for any of the spectral types in question. Therefore, we have combined the data from those two bands in our analysis. In Table 9, we present our estimates of the intrinsic colors of young stars for the bands from 2MASS, *Gaia*, *WISE*, and *Spitzer*. The same values are listed for $K_s - [4.5]$ and $K_s - W2$. Since $[24]$ and $W4$ are similar bands and the $[24]$ observations are more sensitive, the values of $K_s - [24]$ are adopted for $K_s - W4$.

REFERENCES

- Aguado, D. S., Ahumada, R., Almeida, A., et al. 2019, *ApJS*, 240, 23
- Aller, K. M., Kraus, A. L., Liu, M. C., et al. 2013, *ApJ*, 773, 63
- Allers, K. N., & Liu, M. C. 2013, *ApJ*, 772, 79
- Alonso, R., Deeg, H. J., Hoyer, S., et al. 2015, *A&A*, 584, L8
- Andersen, J., & Nordstrom, B. 1983, *A&AS*, 52, 471
- Ansdell, M., Gaidos, E., Rappaport, S. A., et al. 2016, *ApJ*, 816, 69
- Ardila, D., Martín, E., & Basri, G. 2000, *AJ*, 120, 479
- Asensio-Torres, R., Currie, T., Janson, M., et al. 2019, *A&A*, 622, A42
- Bailer-Jones, C. A. L., Rybizki, J., Founesneau, M., Mantelet, G., & Andrae, R. 2018, *AJ*, 156, 58
- Baraffe, I., Chabrier, G., Allard, F., & Hauschildt, P. H. 1998, *A&A*, 337, 403
- Baraffe, I., Horneimer, D., Allard, F., & Chabrier, G. 2015, *A&A*, 577, 42
- Beccari, G., Boffin, H. M. J., Jerabkova, T., et al. 2018, *MNRAS*, 481, L11
- Béjar, V. J. S., Zapatero Osorio, M. R., Pérez-Garrido, A., et al. 2008, *ApJ*, 673, L185
- Bell, C. P. M., Mamajek, E. E., & Naylor, T. 2015, *MNRAS*, 454, 593
- Bell, C. P. M., Murphy, S. J., & Mamajek, E. E. 2017, *MNRAS*, 468, 1198
- Best, W. M. J., Liu, M. C., Magnier, E. A., et al. 2017, *ApJ*, 837, 95
- Billar, B., Allers, K., Liu, M., Close, L. M., & Dupey, T. 2011, *AJ*, 730, 39
- Binks, A. S., & Jeffries, R. D. 2014, *MNRAS*, 438, L11
- Binks, A. S., & Jeffries, R. D. 2016, *MNRAS*, 455, 3345
- Bowler, B. P., Kraus, A. L., Bryan, M. L., et al. 2017, *AJ*, 154, 165
- Bowler, B. P., Liu, M. C., Kraus, A. L., & Mann, A. W. 2014, *ApJ*, 784, 65
- Bowler, B. P., Liu, M. C., Kraus, A. L., Mann, A. W., & Ireland, M. J. 2011, *ApJ*, 743, 148
- Bonnefoy, M., Chauvin, G., Lagrange, A.-M., et al. 2014, *A&A*, 562, A127
- Bouvier, J., & Appenzeller, I. 1992, *A&AS*, 92, 481
- Brandner, W., & Zinnecker, H. 1997, *A&A*, 321, 220
- Bryan, M. L., Bowler, B. P., Knutson, H. A., et al. 2016, *ApJ*, 827, 100
- Byers, S., & Raftery, A. E. 1998, *Journal of the American Statistical Association*, 93, 577
- Cánovas, H., Cantero, C., Cieza, L., et al. 2019, *A&A*, 626, A80
- Carpenter, J. M., Mamajek, E. E., Hillenbrand, L. A., & Meyer, M. R. 2006, *ApJ*, 651, L49
- Carpenter, J. M., Mamajek, E. E., Hillenbrand, L. A., & Meyer, M. R. 2009, *ApJ*, 705, 1646
- Castelli, F., & Kurucz R. L. 2004, *arXiv:astro-ph/0405087*
- Chambers, K. C., Magnier, E. A., Metcalfe, N., et al. 2016, *arXiv:1612.05560*
- Chapman, N. L., Mundy, L. G., Lai, S.-P., & Evans, N. J. 2009, *ApJ*, 690, 496
- Chen, C. H., Mamajek, E. E., Bitner, M. A., et al. 2011, *AJ*, 738, 122
- Chinchilla, P., Béjar, V. J. S., Lodieu, N., et al. 2020, *A&A*, 633, A152
- Chini, R. 1981, *A&A*, 99, 346
- Choi, J., Dotter, A., Conroy, C., et al. 2016, *ApJ*, 823, 102
- Cieza, L. A., Schreiber, M. R., Romero, G. A., et al. 2010, *ApJ*, 712, 925
- Close, L. M., Zuckerman, B., Song, I., et al. 2007, *ApJ*, 660, 1492
- Cody, A. M., Hillenbrand, L. A., David, T. J., et al. 2017, *ApJ*, 836, 41
- Cohen, M., & Kuhl, L. V. 1979, *ApJS*, 41, 743
- Cameron, F. 2008, in *Handbook of Star Forming Regions*, Vol. 2, *The Southern Sky*, ASP Monograph Series 5, ed. B. Reipurth (San Francisco, CA: ASP), 295
- Cook, N. J., Scholz, A., & Jayawardhana, R. 2017, *AJ*, 154, 256
- Corbally, C. J. 1984, *ApJS*, 285, 195
- Cowley, A., Cowley, C., Jaschek, M., & Jaschek, C. 1969, *AJ*, 74, 375
- Cruz, K. L., Reid, I. N., Liebert, J., Kirkpatrick, J. D., & Lowrance, P. J. 2003, *AJ*, 126, 2421
- Cushing, M. C., Rayner, J. T., & Vacca, W. D. 2005, *ApJ*, 623, 1115
- Cushing, M. C., Vacca, W. D., & Rayner, J. T. 2004, *PASP*, 116, 362
- Dahm, S. E., Slesnick, C. L., & White, R. J. 2012, *ApJ*, 745, 56
- Damiani, F., Prisinzano, L., Pillitteri, I., Micela, G., & Sciortino, S. 2019, *A&A*, 623, A112
- Da Rio, N., Robberto, M., Hillenbrand, L. A., Henning, T., & Stassun, K. G. 2012, *ApJ*, 748, 14
- David, T. J., Hillenbrand, L. A., Cody, A. M., Carpenter, J. M., & Howard, A. W. 2016a, *ApJ*, 816, 21
- David, T. J., Hillenbrand, L. A., Gillen, E., et al. 2019, *ApJ*, 872, 161
- David, T. J., Hillenbrand, L. A., Petigura, E. A., et al. 2016b, *Nature*, 534, 658
- David, T. J., Petigura, E. A., Hillenbrand, L. A., et al. 2017, *ApJ*, 835, 168
- Dawson, P., Scholz, A., Ray, T. P., et al. 2013, *MNRAS*, 429, 903
- Dawson, P., Scholz, A., Ray, T. P., et al. 2014, *MNRAS*, 442, 1586
- de Bruijne, J. H. J. 2012, *Ap&SS*, 341, 31
- de Geus, E. J., de Zeeuw, P. T., & Lub, J. 1989, *A&A*, 216, 44
- de Zeeuw, P. T., Hoogerwerf, R., de Bruijne, J. H. J., Brown, A. G. A., & Blaauw, A. 1999, *AJ*, 117, 354
- Dobbie, P. D., Lodieu, N., & Sharp, R. G. 2010, *MNRAS*, 409, 1002
- Donaldson, J. K., Weinberger, A. J., Gagné, J., Boss, A. P., & Keiser, S. A. 2017, *ApJ*, 850, 11
- Dotter, A. 2016, *ApJS*, 222, 8
- Ducati, J. R. 2002, *yCat*, 2237, 0
- Durkan, S., Janson, M., Ciceri, S., et al. 2018, *A&A*, 618, 5
- Dzib, S. A., Loinard, L., Ortis-León, G. N., Rodríguez, L. F., & Galli, P. A. B. 2018, *ApJ*, 867, 151
- Eikenberry, S., Albert, L., Forveille, T., et al. 2004, *Proc. SPIE*, 5492, 1196
- Eisner, J. A., Hillenbrand, L. A., White, R. J., Akeson, R. L., & Sargent, A. I. 2005, *ApJ*, 623, 952
- Elias, J. H., Joyce, R. R., Liang, M., et al. 2006, *Proc. SPIE*, 6269, 62694C
- Epchtein, N., Deul, E., Derriere, S., et al. 1999, *A&A*, 349, 236
- Espaillet, C., Ingleby, L., Hernandez, J., et al. 2012, *ApJ*, 747, 103
- Esplin, T. L., & Luhman, K. L. 2019, *AJ*, 158, 54
- Esplin, T. L., & Luhman, K. L. 2020, *AJ*, in press
- Esplin, T. L., Luhman, K. L., Faherty, J. K., Mamajek, E. E., & Bochanski, J. J. 2017, *AJ*, 154, 46
- Esplin, T. L., Luhman, K. L., & Mamajek, E. E. 2014, *ApJ*, 784, 126
- Esplin, T. L., Luhman, K. L., Miller, E. B., & Mamajek, E. E. 2018, *AJ*, 156, 75
- Evans, D. W., Riello, M., De Angeli, F., et al. 2018, *A&A*, 616, A4
- Faherty, J. K., Bochanski, J. J., Gagné, J., et al. 2018, *ApJ*, 863, 91
- Faherty, J. K., Riedel, A. R., Cruz, K. L., et al. 2016, *ApJS*, 225, 10
- Fazio, G. G., Hora, J. L., Allen, L. E., et al. 2004, *ApJS*, 154, 10
- Feiden, G. A. 2016, *A&A*, 593, A99
- Fitzpatrick, E. L., & Massa, D. 2007, *ApJ*, 663, 320
- Flewelling, H. A., Magnier, E. A., Chambers, K. C., et al. 2016, *arXiv:1612.05243*
- Gagné, J., & Faherty, J. K. 2018, *ApJ*, 862, 138
- Gagné, J., Faherty, J. K., Cruz, K. L., et al. 2014, *ApJ*, 785, L14
- Gagné, J., Faherty, J. K., Mamajek, E. E., et al. 2017, *ApJS*, 228, 18
- Gagné, J., Mamajek, E. E., Malo, L., et al. 2018, *ApJ*, 856, 23
- Gagné, J., Roy-Loubier, O., Faherty, J. K., Doyon, R., & Malo, L. 2018, *ApJ*, 860, 43
- Gaia Collaboration, Babusiaux, C., van Leeuwen, F., Barstow, M. A., et al. 2018a, *A&A*, 616, A10
- Gaia Collaboration, Brown, A. G. A., Vallenari, A., et al. 2016, *A&A*, 595, A2
- Gaia Collaboration, Brown, A. G. A., Vallenari, A., Prusti, T., et al. 2018b, *A&A*, 616, A1
- Gaia Collaboration, Lindgren, L., Hernández, J., Bombrun, A., et al. 2018c, *A&A*, 616, A2

- Gaia Collaboration, Prusti, T., de Bruijne, J. H. J., et al. 2016b, *A&A*, 595, A1
- Galli, P. A. B., Bouy, H., Olivares, J., et al. 2020, *A&A*, 634, A98
- Galli, P. A. B., Joncour, I., & Moraux, E. 2018, *MNRAS*, 477, L50
- Garrison, R. F. 1967, *ApJ*, 147, 1003
- Gizis, J. E. 2002, *ApJ*, 575, 484
- Goldman, B., Röser, S., Schilbach, E., Moór, A. C., & Henning, T. 2018, *ApJ*, 868, 32
- Gontcharov, G. A. 2006, *AstL*, 32, 759
- Gray, R. O., Corbally, C., Garrison, R. F., et al. 2006, *AJ*, 132, 161
- Henry, T. J., Kirkpatrick, J. D., & Simons, D. A. 1994, *AJ*, 108, 1437
- Herczeg, G. J., Cruz, K. L., & Hillenbrand, L. A. 2009, *ApJ*, 696, 1589
- Herczeg, G. J., & Hillenbrand, L. A. 2014, *ApJ*, 786, 97
- Herczeg, G. J., & Hillenbrand, L. A. 2015, *ApJ*, 808, 23
- Herczeg, G. J., Kuhn, M. A., Zhou, X., et al. 2019, *ApJ*, 878, 111
- Hillenbrand, L. A. 1997, *AJ*, 113, 1733
- Hillenbrand, L. A., Hoffer, A. S., & Herczeg, G. J. 2013, *AJ*, 146, 85
- Hiltner, W. A., Garrison, R. F., & Schild, R. E. 1969, *ApJ*, 157, 313
- Hodgkin, S. T., Irwin, M. J., Hewett, P. C., & Warren, S. J. 2009, *MNRAS*, 394, 675
- Houk, N. 1982, *Michigan Catalogue of Two-dimensional Spectral Types for the HD Stars. Vol. 3*, (Ann Arbor: Univ. Mich.)
- Houk, N., & Smith-Moore, M. 1988, *Michigan Catalogue of Two-dimensional Spectral Types for the HD Stars. Vol. 4*, (Ann Arbor: Univ. Mich.)
- Inebetouw, R., Mathis, J. S., Babler, B. L., et al. 2005, *ApJ*, 619, 931
- Ireland, M. J., Kraus, A., Martinache, F., Law, N., & Hillenbrand, L. A. 2011, *ApJ*, 726, 113
- Jayawardhana, R., & Ivanov, V. D. 2006, *ApJ*, 647, L167
- Jilinski, E., Daflon, S., Cunha, K., & de La Reza, R. 2006, *A&A*, 448, 1001
- Johnson D. R. H., & Soderblom D. R., 1987, *AJ*, 93, 864
- Kaiser, N., Aussel, H., Burke, B. E., et al. 2002, *Proc. SPIE*, 4836, 154
- Kaiser, N., Burgett, W., Chambers, K., et al. 2010, *Proc. SPIE*, 7733, 12
- Kellogg, K., Metchev, S., Geiffler, K., et al. 2015, *AJ*, 150, 182
- Kenyon, S. J., & Hartmann, L. 1995, *ApJS*, 101, 117
- Kirkpatrick, J. D., Henry, T. J., & Irwin, M. J. 1997, *AJ*, 113, 1421
- Kirkpatrick, J. D., Henry, T. J., & McCarthy, D. W. 1991, *ApJS*, 77, 417
- Kirkpatrick, J. D., Looper, D. L., Burgasser, A. J., et al. 2010, *ApJS*, 190, 100
- Kraus, A. L., Cody, A. M., Covey, K. R., et al. 2015, *ApJ*, 807, 3
- Kraus, A. L., & Hillenbrand, L. A. 2007, *ApJ*, 664, 1167
- Kraus, A. L., & Hillenbrand, L. A. 2009, *ApJ*, 703, 1511
- Kraus, A. L., Ireland, M. J., Cieza, L. A., et al. 2014, *ApJ*, 781, 20
- Kuhn, M. A., Hillenbrand, L. A., Sills, A., Feigelson, E. D., & Getman, K. V. 2019, *ApJ*, 870, 32
- Kunder, A., Kordopatis, G., Steinmetz, M., et al. 2017, *AJ*, 153, 75
- Kunkel, M. 1999, Ph.D. thesis, Julius-Maximilians-Univ., Würzburg
- Kurosawa, R., Harries, T. J., & Littlefair, S. P. 2006, *MNRAS*, 372, 1879
- Lachapelle, F.-R., Lafrenière, D., Gagné, J., et al. 2015, *ApJ*, 802, 61
- Lafrenière, D., Jayawardhana, R., Janson, M., et al. 2011, *ApJ*, 730, 42
- Lafrenière, D., Jayawardhana, R., & van Kerkwijk, M. H. 2008, *ApJ*, 689, L153
- Lawrence, A., Warren, S. J., Almaini, O., et al. 2007, *MNRAS*, 379, 1599
- Lindgren, L. 2018, Re-normalising the astrometric chi-square in Gaia DR2, GAIA-C3-TN-LU-LL-124-01, http://www.rssd.esa.int/doc_fetch.php?id=3757412
- Lodieu, N. 2013, *MNRAS*, 431, 3222
- Lodieu, N., Alonso, R., González Hernández, J. I., et al. 2015, *A&A*, 584, A128
- Lodieu, N., Dobbie, P. D., & Hambly, N. C. 2011a, *A&A*, 527, A24
- Lodieu, N., Hambly, N. C., & Jameson, R. F. 2006, *MNRAS*, 373, 95
- Lodieu, N., Hambly, N. C., Jameson, R. F., & Hodgkin, S. T. 2008, *MNRAS*, 383, 1385
- Lodieu, N., Zapatero Osorio, M. R., Béjar, V. J. S., & Peña Ramírez, K. 2018, *MNRAS*, 473, 2020
- Looper, D. L., Bochanski, J. J., Burgasser, A. J., et al. 2010b, *AJ*, 140, 1486
- Looper, D. L., Burgasser, A. J., Kirkpatrick, J. D., & Swift, B. J. 2007, *ApJ*, 669, L97
- Looper, D. L., Mohanty, S., & Bochanski, J. J., 2010a, *ApJ*, 714, 45
- Lucas, P. W., Roche, P. F., Allard, F., & Hauschildt, P. H. 2001, *MNRAS*, 326, 695
- Luhman, K. L. 1999, *ApJ*, 525, 466
- Luhman, K. L. 2005, *ApJ*, 633, L41
- Luhman, K. L. 2018, *AJ*, 156, 271
- Luhman, K. L., Adame, L., D'Alessio, P., et al. 2007, *ApJ*, 666, 1219
- Luhman, K. L., Allen, P. R., Espaillat, C., Hartmann, L., & Calvet, N. 2010, *ApJS*, 186, 111
- Luhman, K. L., Allers, K. N., Jaffe, D. T., et al. 2007, *ApJ*, 659, 1629
- Luhman, K. L., Esplin, T. L., & Loutrel, N. P. 2016, *ApJ*, 827, 52
- Luhman, K. L., Herrmann, K. A., Mamajek, E. E., Esplin, T. L., & Pecaut, M. J. 2018, *AJ*, 156, 76
- Luhman, K. L., Liebert, J., & Rieke, G. H. 1997, *ApJ*, 489, L165
- Luhman, K. L., & Mamajek, E. E. 2012, *ApJ*, 758, 31
- Luhman, K. L., Mamajek, E. E., Shukla, S. J., & Loutrel, N. P. 2017, *AJ*, 153, 46
- Luhman, K. L., & Steeghs, D. 2004, *ApJ*, 609, 917
- Lutz, T. E., & Lutz, J. H. 1977, *AJ*, 82, 431
- Lyo, A., Lawson, W. A., & Bessell, M. S. 2004, *MNRAS*, 355, 363
- MacDonald, J., & Mullan, D. J. 2017, *ApJ*, 834, 67
- Mace, G. N., Prato, L., Torres, G., et al. 2012, *AJ*, 144, 55
- Maíz Apellániz, J., & Weiler, M. 2018, *A&A*, 619, A180
- Majewski, S. R., Schiavon, R. P., Frinchaboy, P. M., et al. 2017, *AJ*, 154, 94
- Mamajek, E. E. 2007, in *IAU Symp. 237, Triggered Star Formation in a Turbulent ISM*, ed. B. G. Elmegreen & J. Palous (Cambridge: Cambridge Univ. Press), 442
- Mamajek, E. E., & Bell, C. P. M. 2014, *MNRAS*, 445, 2169
- Mamajek, E. E., Lawson, W. A., & Feigelson, E. D. 1999, *ApJ*, 516, L77
- Mann, A. W., Newton, E. R., Rizzuto, A. C., et al. 2016, *AJ*, 152, 61
- Mann, A. W., & von Braun, K. 2015, *PASP*, 127, 102
- Martín, E. L. 1998, *AJ*, 115, 351
- Martín, E. L., Delfosse, X., & Guieu, S. 2004, *AJ*, 127, 449
- Martín, E. L., Montmerle, T., Gregorio-Hetem, J., & Casanova, S. 1998, *MNRAS*, 300, 733
- Martín, E. L., Phan-Bao, N., Bessell, M., et al. 2010, *A&A*, 517, A53
- Martini, P., Stoll, R., Derwent, M. A., et al. 2011, *PASP*, 123, 187
- McClure, M. K., Furlan, E., Manoj, P., et al. 2010, *ApJS*, 188, 75
- McMahon, R. G., Banerji, M., Gonzalez, E., et al. 2013, *The Messenger*, 154, 35
- Merín, B., Brown, J. M., Oliveira, I., et al. 2010, *ApJ*, 718, 1200
- Mora, A., Merin, B., Solano, E., et al. 2001, *A&A*, 378, 116
- Murphy, R. E. 1969, *AJ*, 74, 1082
- Muzerolle, J., Hillenbrand, L., Calvet, N., Briceño, C., & Hartmann, L. 2003, *ApJ*, 592, 266
- Oh, S., Price-Whelan, A. M., Hogg, D. W., Morton, T. D., & Spergel, D. N. 2017, *AJ*, 153, 257
- Pecaut, M. J., & Mamajek E. E. 2013, *ApJS*, 208, 9
- Pecaut, M. J., & Mamajek E. E. 2016, *MNRAS*, 461, 794
- Pecaut, M. J., Mamajek E. E., & Bubar E. J. 2012, *ApJ*, 746, 154
- Peña Ramírez, K., Béjar, V. J. S., & Zapatero Osorio, M. R. 2016, *A&A*, 586, A157
- Perryman, M. A. C., de Boer, K. S., Gilmore, G., et al. 2001, *A&A*, 369, 339
- Prato, L. 2007, *ApJ*, 657, 338
- Prato, L., Greene, T. P., & Simon, M. 2003, *ApJ*, 584, 853
- Prato, L., Simon, M., Mazeh, T., et al. 2002, *ApJ*, 569, 863

- Preibisch, T., Brown, A. G. A., Bridges, T. Guenther, E., & Zinnecker, H. 2002, *AJ*, 124, 404
- Preibisch, T., Guenther, E., & Zinnecker, H. 2001, *AJ*, 121, 1040
- Preibisch, T., Guenther, E., Zinnecker, H., et al. 1998, *A&A*, 333, 619
- Preibisch, T., & Mamajek, E. 2008, in *Handbook of Star Forming Regions*, Vol. 2, *The Southern Sky*, ASP Monograph Series 5, ed. B. Reipurth (San Francisco, CA: ASP), 235
- Price-Whelan, A. 2018, doi:10.5281/zenodo.1228136
- R Core Team, 2013, R Foundation for Statistical Computing, Vienna, Austria, [\protecthttp://www.R-project.org](http://www.R-project.org)
- Rayner, J. T., Cushing, M. C., & Vacca, W. D. 2009, *ApJS*, 185, 289
- Rayner, J. T., Toomey, D. W., Onaka, P. M., et al. 2003, *PASP*, 115, 362
- Reggiani, M., Robberto, M., Da Rio, N., et al. 2011, *A&A*, 534, A83
- Reid, I. N., Cruz, K. L., Kirkpatrick, J. D., et al. 2008, *AJ*, 136, 1290
- Reis, W., Corradi, W., de Avillez, M. A., & Santos, F. P. 2011, *ApJ*, 734, 8
- Riaz, B., Gizis, J. E., & Harvin, J. 2006, *AJ*, 132, 866
- Riaz, B., Lodieu, N., Goodwin, S., Stamatellos, D., & Thompson, M. 2012, *MNRAS*, 420, 2497
- Rice, E. L., Barman, T., McLean, I. S., Prato, L., & Kirkpatrick, J. D. 2010, *ApJS*, 186, 63
- Rieke, G. H., Young, E. T., Engelbracht, C. W., et al. 2004, *ApJS*, 154, 25
- Rizzuto, A. C., Ireland, M. J., & Kraus, A. L. 2015, *MNRAS*, 448, 2737
- Rizzuto, A. C., Ireland, M. J., & Zucker, D. B. 2012, *MNRAS*, 421, L97
- Roccatagliata, V., Sacco, G. G., Franciosini, E., & Randich, S. 2018, *A&A*, 617, L4
- Romero, G. A., Schreiber, M. R., Cieza, L. A., et al. 2012, *ApJ*, 749, 79
- Röser, S., Schilbach, E., Goldman, B., et al. 2018, *A&A*, 614, A18
- Ruiz, M. T., Maza, J., Gonzalez, L. E., & Wischnjewsky, M. 1987, *AJ*, 94, 1299
- Schlafly, E. F., Meisner, A. M., Stutz, A. M., et al. 2016, *ApJ*, 821, 78
- Schneider, A. C., Windsor, J., Cushing, M. C., Kirkpatrick, J. D., & Wright, E. L. 2016, *ApJ*, 822, L1
- Scholz, R.-D., McCaughrean, M. J., Zinnecker, H., & Lodieu, N. 2005, *A&A*, 430, L49
- Shkolnik, E., Allers, K. N., Kraus, A. L., Liu, M. C. & Flagg, L. 2017, *AJ*, 154, 69
- Shkolnik, E., Liu, M. C., & Reid, I. N. 2009, *ApJ*, 699, 649
- Shkolnik, E. L., Liu, M. C., Reid, I. N., Dupuy, T., & Weinberger, A. J. 2011, *ApJ*, 727, 6
- Schlieder, J. E., Lépine, S., & Simon, M. 2010, *AJ*, 140, 119
- Schlieder, J. E., Lépine, S., & Simon, M. 2012, *AJ*, 144, 109
- Schneider, A., Song, I., Melis, C., Zuckerman, B., & Bessell, M. 2012, *ApJ*, 757, 163
- Scrucca L., Fop M., Murphy T. B., & Raftery A. E. 2016, *mclust* 5: clustering, classification and density estimation using Gaussian finite mixture models, *The R Journal*, 8, 205
- Shvonski, A. J., Mamajek, E. E., Kim, J. S., Meyer, M. R., & Pecauc, M. J. 2016, arXiv:1612.06924
- Simcoe, R. A., Burgasser, A. J., Schechter, P. L., et al. 2013, *PASP*, 125, 270
- Skrutskie, M., Cutri, R. M., Stiening, R., et al. 2006, *AJ*, 131, 1163
- Slesnick, C. L., Carpenter, J. M., & Hillenbrand, L. A. 2006, *AJ*, 131, 3016
- Slesnick, C. L., Hillenbrand, L. A., & Carpenter, J. M., 2008, *ApJ*, 688, 377
- Soderblom D. R., Hillenbrand L. A., Jeffries R. D., Mamajek E. E., & Naylor T., 2014, *Protostars and Planets VI*. Univ. Arizona Press, Tucson, AZ, 219
- Song, I., Zuckerman, B., & Bessell, M. S. 2012, *AJ*, 144, 8
- Stauffer, J., Collier-Cameron, A., Jardine, M., et al. 2017, *AJ*, 153, 152
- Stauffer, J., Rebull, L., David, T. J., et al. 2018, *AJ*, 155, 63
- Sterzik, M. F., Alcalá, J. M., Covino, E., & Petr, M. G. 1999, *A&A*, 346, L41
- Torres, C. A. O., Quast, G. R., Da Silva, L., et al. 2006, *A&A*, 460, 695
- Tucker, B. E., Freeman, K., Yuan, F., et al. 2015, *ATel*, 7996, 1T
- Vacca, W. D., Cushing, M. C., & Rayner, J. T. 2003, *PASP*, 115, 389
- van der Blik, N. S., Manfroid, J., & Bouchet, P. 1996, *A&AS*, 119, 547
- Venables, W. N., & Ripley, B. D. 2002, *Modern Applied Statistics with S*. Fourth Edition. Springer, New York
- Vieira, S. L. A., Corradi, W. J. B., Alencar, S. H. P., et al. 2003, *AJ*, 126, 2971
- Walter, F. M., Vrba, F. J., Mathieu, R. D., Brown, A., & Myers, P. C. 1994, *AJ*, 107, 692
- Wang, J., David, T. J., Hillenbrand, L. A., et al. 2018, *ApJ*, 865, 141
- Webb, R. A., Zuckerman, B., Platais, I., et al. 1999, *ApJ*, 512, L63
- Werner, M. W., Roellig, T. L., Low, F. J., et al. 2004, *ApJS*, 154, 1
- White, R. J., Gabor, J. M., & Hillenbrand, L. A. 2007, *AJ*, 133, 2524
- Wilkinson, S., Merín, B., & Riviere-Marichalar, P. 2018, *A&A*, 618, A12
- Wright, E. L., Eisenhardt, P. R., Mainzer, A. K., et al. 2010, *AJ*, 140, 1868
- Wright, N. J., Jeffries, R. D., Jackson, R. J., et al. 2019, *MNRAS*, 486, 2477
- Wright, N. J., & Mamajek, E. E. 2018, *MNRAS*, 476, 381
- Zuckerman, B., & Song, I. 2004, *ARA&A*, 42, 685
- Zuckerman, B., Song, I., Bessell, M. S., & Webb, R. A. 2001, *ApJ*, 562, L87

TABLE 1
CANDIDATE MEMBERS OF UPPER SCO

Column Label	Description
2MASS	2MASS Point Source Catalog source name
WISEA	AllWISE Source Catalog source name
UGCS	UKIDSS Galactic Clusters Survey source name ^a
Gaia	<i>Gaia</i> DR2 source name
RAdeg	Right Ascension (J2000)
DEdeg	Declination (J2000)
Ref-Pos	Reference for right ascension and declination ^b
SpType	Spectral type
r_SpType	Spectral type reference ^c
pmRA	Proper motion in right ascension from <i>Gaia</i> DR2
e_pmRA	Error in pmRA
pmDec	Proper motion in declination from <i>Gaia</i> DR2
e_pmDec	Error in pmDec
plx	Parallax from <i>Gaia</i> DR2
e_plx	Error in plx
Gmag	<i>G</i> magnitude from <i>Gaia</i> DR2
e_Gmag	Error in Gmag
GBPmag	<i>G</i> _{BP} magnitude from <i>Gaia</i> DR2
e_GBPmag	Error in GBPmag
GRPmag	<i>G</i> _{RP} magnitude from <i>Gaia</i> DR2
e_GRPmag	Error in GRPmag
RUWE	renormalized unit weight error from Lindegren (2018)
Jmag	<i>J</i> magnitude
e_Jmag	Error in Jmag
Hmag	<i>H</i> magnitude
e_Hmag	Error in Hmag
Ksmag	<i>K</i> _s magnitude
e_Ksmag	Error in Ksmag
JHKref	<i>JHK</i> _s reference ^d
selection	Selection criteria satisfied by candidate ^e
separation	Angular separation from nearest known young star within 5''
compGaia	<i>Gaia</i> DR2 source name of nearest known young star within 5''

NOTE. — The table is available in its entirety in machine-readable form.

^a Based on coordinates from DR10 of the UKIDSS Galactic Clusters Survey for stars with $K_s > 10$ from 2MASS.

^b Sources of the right ascension and declination are DR2 of *Gaia*, DR10 of the UKIDSS Galactic Clusters Survey, DR6 of VISTA VHS, and the 2MASS Point Source Catalog.

^c (1) Houk & Smith-Moore (1988); (2) Houk (1982); (3) this work; (4) Luhman et al. (2018).

^d 2 = 2MASS Point Source Catalog; u = UKIDSS Galactic Clusters Survey DR10; v = VISTA VHS DR6.

^e G/W/i/Y/Z/ip/zp/yp = CMDs in Luhman et al. (2018); pi = parallax from *Gaia* DR2; gaia/gps/ucac/2m-gaia/2m-ps/ukidss = proper motions in Luhman et al. (2018) and this work.

TABLE 2
OBSERVING LOG

Telescope/Instrument ^a	Disperser/Aperture	Wavelengths/Resolution	Targets
Bok Reflector/B&C	600 l mm ⁻¹ /1''5 slit	0.63–0.86 μm/5 Å	24
CTIO 4 m/COSMOS	red VPH/1''2 slit	0.55–0.95 μm/4 Å	177
Gemini North/GNIRS	31.7 l mm ⁻¹ /1'' slit	0.9–2.5 μm/R=600	46
Gemini South/FLAMINGOS-2	HK grism/0''72 slit	1.10–2.65 μm/R=450	3
Magellan Baade/FIRE	prism/0''8 slit	0.8–2.5 μm/R=300	3
IRTF/SpEX	prism/0''8 slit	0.8–2.5 μm/R=150	179

^a The Gemini Near-Infrared Spectrograph (GNIRS), FLAMINGOS-2, the Folded-Port Infrared Echellette (FIRE), and SpeX are described by Elias et al. (2006), Eikenberry et al. (2004), Simcoe et al. (2013), and Rayner et al. (2003), respectively. The Cerro Tololo Ohio State Multi-Object Spectrograph (COSMOS) is based on an instrument described by Martini et al. (2011).

TABLE 3
SPECTROSCOPIC DATA FOR CANDIDATE MEMBERS OF UPPER SCO

Source Name ^a	Spectral Type ^b	$W_\lambda(\text{Li})^c$ (Å)	Instrument	Date	Young?
Gaia 6261607772589226496	M1.5	0.50	COSMOS	2018 May 31	Y
Gaia 6234768006561947520	K5	0.35	COSMOS	2018 May 31	Y
Gaia 6234796284628451968	M8	...	GNIRS	2018 Mar 5	N?
Gaia 6234811166691211008	M5	...	SpeX	2019 Apr 25	Y
UGCS J154519.90–261653.3	M8–L0	...	GNIRS	2018 Mar 14	Y

NOTE. — The table is available in its entirety in machine-readable form.

^a Source names are from DR2 of *Gaia*, DR10 of the UKIDSS Galactic Clusters Survey, and the 2MASS Point Source Catalog.

^b Uncertainties are 0.25 and 0.5 subclass for optical and IR spectral types, respectively, unless indicated otherwise.

^c Typical uncertainties are 0.05 Å.

TABLE 4
YOUNG STARS TOWARD UPPER SCO

Column Label	Description
2MASS	2MASS Point Source Catalog source name
WISEA	AllWISE Source Catalog source name ^a
UGCS	UKIDSS Galactic Clusters Survey source name ^b
Gaia	<i>Gaia</i> DR2 source name
Name	Other source name
RAdeg	Right Ascension (J2000)
DEdeg	Declination (J2000)
Ref-Pos	Reference for right ascension and declination ^c
SpType	Spectral type
r_SpType	Spectral type reference ^d
Adopt	Adopted spectral type
Ak	Extinction in K_s
f_Ak	Method of extinction estimation ^e
pmRA	Proper motion in right ascension from <i>Gaia</i> DR2
e_pmRA	Error in pmRA
pmDec	Proper motion in declination from <i>Gaia</i> DR2
e_pmDec	Error in pmDec
plx	Parallax from <i>Gaia</i> DR2
e_plx	Error in plx
RVel	Radial velocity
e_RVel	Error in RVel
r_RVel	Radial velocity reference ^f
U	U component of space velocity
e_U	Error in U
V	V component of space velocity
e_V	Error in V
W	W component of space velocity
e_W	Error in W
Gmag	G magnitude from <i>Gaia</i> DR2
e_Gmag	Error in Gmag
GBPmag	G_{BP} magnitude from <i>Gaia</i> DR2
e_GBPmag	Error in GBPmag
GRPmag	G_{RP} magnitude from <i>Gaia</i> DR2
e_GRPmag	Error in GRPmag
RUWE	renormalized unit weight error from Lindegren (2018)
Jmag	J magnitude
e_Jmag	Error in Jmag
Hmag	H magnitude
e_Hmag	Error in Hmag
Ksmag	K_s magnitude
e_Ksmag	Error in Ksmag
JHKref	JHK_s reference ^g
Pops	<i>Gaia</i> parallax and proper motion consistent with these populations ^h
USco	Adopted member of Upper Sco?

TABLE 4 — *Continued*

Column Label	Description
--------------	-------------

NOTE. — The table is available in its entirety in machine-readable form.

^a The following names are from the WISE All-Sky Source Catalog: J160027.15–223850.5, J160414.16–212915.5, J161320.78–175752.3, J161317.38–292220.0, J161837.22–240522.8, J162210.14–240905.4, J162620.15–223312.8.

^b Based on coordinates from DR10 of the UKIDSS Galactic Clusters Survey for stars with $K_s > 10$ from 2MASS.

^c Sources of the right ascension and declination are DR2 of *Gaia*, DR10 of the UKIDSS Galactic Clusters Survey, DR6 of VISTA VHS, the 2MASS Point Source Catalog, and high-resolution imaging (Ireland et al. 2011; Lachapelle et al. 2015; Bryan et al. 2016).

^d (1) Houk & Smith-Moore (1988); (2) Luhman et al. (2018); (3) Kunkel (1999); (4) Preibisch et al. (1998); (5) Pecaut & Mamajek (2016); (6) Hiltner et al. (1969); (7) this work; (8) Torres et al. (2006); (9) Esplin et al. (2018); (10) Rizzuto et al. (2015); (11) Dawson et al. (2014); (12) Lodieu et al. (2006); (13) Lodieu et al. (2008); (14) Bonnefoy et al. (2014); (15) Ruiz et al. (1987); (16) Best et al. (2017); (17) Vieira et al. (2003); (18) Peña Ramírez et al. (2016); (19) Houk (1982); (20) Pecaut et al. (2012); (21) Corbally (1984); (22) Shkolnik et al. (2009); (23) Cruz et al. (2003); (24) measured in this work with the most recently published spectrum; (25) Aller et al. (2013); (26) Ardila et al. (2000); (27) Martín et al. (2004); (28) Walter et al. (1994); (29) Martín et al. (2010); (30) Kraus & Hillenbrand (2009); (31) Slesnick et al. (2008); (32) Chinchilla et al. (2020); (33) Preibisch et al. (2002); (34) Mora et al. (2001); (35) Reid et al. (2008); (36) Kirkpatrick et al. (2010); (37) Allers & Liu (2013); (38) Faherty et al. (2016); (39) Gizis (2002); (40) Herczeg & Hillenbrand (2014); (41) Slesnick et al. (2006); (42) Riaz et al. (2006); (43) Lodieu et al. (2018); (44) Kraus et al. (2015); (45) Mace et al. (2012); (46) Cody et al. (2017); (47) Lafrenière et al. (2011); (48) Lachapelle et al. (2015); (49) Preibisch et al. (2001); (50) David et al. (2019); (51) Ansdell et al. (2016); (52) Prato et al. (2002); (53) Béjar et al. (2008); (54) Herczeg et al. (2009); (55) Kraus & Hillenbrand (2007); (56) Lodieu et al. (2011a); (57) Asensio-Torres et al. (2019); (58) Biller et al. (2011); (59) Lafrenière et al. (2008); (60) Luhman et al. (2017); (61) Mann et al. (2016); (62) David et al. (2016b); (63) Stauffer et al. (2017); (64) Stauffer et al. (2018); (65) Cohen & Kuhl (1979); (66) Prato et al. (2003); (67) Eisner et al. (2005); (68) Garrison (1967); (69) Murphy (1969); (70) Martín et al. (1998); (71) Prato (2007); (72) Cowley et al. (1969); (73) McClure et al. (2010); (74) Lodieu et al. (2015); (75) David et al. (2016a); (76) Luhman (2005); (77) Martín (1998); (78) Esplin & Luhman (2020); (79) Gray et al. (2006); (80) Lutz & Lutz (1977); (81) Cieza et al. (2010); (82) Bowler et al. (2011); (83) Bowler et al. (2014); (84) Romero et al. (2012); (85) Jayawardhana & Ivanov (2006); (86) Close et al. (2007); (87) Luhman et al. (2007); (88) Merín et al. (2010); (89) David et al. (2017); (90) Tucker et al. (2015); (91) Brandner et al. (1997); (92) Bouvier & Appenzeller (1992); (93) Bowler et al. (2017).

^e Extinction estimated from a near-IR spectrum or the indicated color assuming the intrinsic spectrum from Luhman et al. (2017) or the intrinsic color from the Appendix for the spectral type in question.

^f (1) Dahm et al. (2012); (2) *Gaia* DR2; (3) Jilinski et al. (2006); (4) Gontcharov (2006); (5) Torres et al. (2006); (6) Chen et al. (2011). (7) Kurosawa et al. (2006); (8) Kunder et al. (2017); (9) Durkan et al. (2018); (10) Andersen & Nordstrom (1983); (11) Muzerolle et al. (2003); (12) David et al. (2016a); (13) White et al. (2007); (14) Mace et al. (2012); (15) Prato et al. (2002); (16) Rice et al. (2010); (17) Alonso et al. (2015); (18) David et al. (2016b); (19) Eisner et al. (2005); (20) Wang et al. (2018); (21) David et al. (2017).

^g 2 = 2MASS Point Source Catalog; u = UKIDSS Galactic Clusters Survey DR10; v = VISTA VHS DR6; van = van der Bliëk et al. (1996); duc = Ducati (2002); luh = Luhman et al. (2007); bow = Bowler et al. (2011); kra = Kraus et al. (2014); lac = Lachapelle et al. (2015).

^h O/o = Ophiuchus; U/u = Upper Sco; S/s = remainder of Sco-Cen; n = none of those populations. Upper case letters indicate that both proper motion and parallax support membership in that population. Lower case letters indicate that either proper motion or parallax supports membership while the other parameter is inaccurate, unreliable, or unavailable.

TABLE 5
MID-IR PHOTOMETRY FOR ADOPTED MEMBERS OF UPPER SCO

Column Label	Description
2MASS	2MASS Point Source Catalog source name
WISEA	AllWISE Source Catalog source name
UGCS	UKIDSS Galactic Clusters Survey source name
Gaia	<i>Gaia</i> DR2 source name
Name	Other source name
RAdeg	Right Ascension (J2000)
DEdeg	Declination (J2000)
Ref-Pos	Reference for right ascension and declination
3.6mag	<i>Spitzer</i> [3.6] magnitude
e.3.6mag	Error in 3.6mag
f.3.6mag	Flag on 3.6mag ^a
4.5mag	<i>Spitzer</i> [4.5] magnitude
e.4.5mag	Error in 4.5mag
f.4.5mag	Flag on 4.5mag ^a
5.8mag	<i>Spitzer</i> [5.8] magnitude
e.5.8mag	Error in 5.8mag
f.5.8mag	Flag on 5.8mag ^a
8.0mag	<i>Spitzer</i> [8.0] magnitude
e.8.0mag	Error in 8.0mag
f.8.0mag	Flag on 8.0mag ^a
24mag	<i>Spitzer</i> [24] magnitude
e.24mag	Error in 24mag
f.24mag	Flag on 24mag ^a
W1mag	<i>WISE</i> W1 magnitude
e.W1mag	Error in W1mag
f.W1mag	Flag on W1mag ^a
W2mag	<i>WISE</i> W2 magnitude
e.W2mag	Error in W2mag
f.W2mag	Flag on W2mag ^a
W3mag	<i>WISE</i> W3 magnitude
e.W3mag	Error in W3mag
f.W3mag	Flag on W3mag ^a
W4mag	<i>WISE</i> W4 magnitude
e.W4mag	Error in W4mag
f.W4mag	Flag on W4mag ^a
Exc4.5	Excess present in [4.5]?
Exc8.0	Excess present in [8.0]?
Exc24	Excess present in [24]?
ExcW2	Excess present in W2?
ExcW3	Excess present in W3?
ExcW4	Excess present in W4?
DiskType	Disk Type

NOTE. — This table is available in its entirety in a machine-readable form.

^a nodet = non-detection; sat = saturated; out = outside of the camera's field of view; bl = photometry may be affected by blending with a nearby star; ext = photometry is known or suspected to be contaminated by extended emission (no data given when extended emission dominates); dif = photometry may be affected by a diffraction spike; bin = includes an unresolved binary companion; unres = too close to a brighter star to be detected; false = detection from WISE catalog appears false or unreliable based on visual inspection; off = W3 and/or W4 detection appears offset from the W1/W2 detection (no data given when offset is due to a known source); err = W2 magnitudes brighter than ~6 are erroneous.

TABLE 6
EXCESS FRACTIONS IN UPPER SCO

Spectral Type	Mass ^a (M_{\odot})	[4.5]/W2	[8.0]	W3	[24]/W4
Full, Transitional, and Evolved Disks					
B0–B8	2.8–18	0/21=<0.08	0/18=<0.09	0/22=<0.08	0/23=<0.07
B8–A6	1.8–2.8	1/47=0.02 ^{+0.05} _{-0.01}	0/29=<0.06	2/49=0.04 ^{+0.05} _{-0.01}	2/49=0.04 ^{+0.05} _{-0.01}
A6–F4	1.5–1.8	0/17=<0.10	0/5=<0.27	4/21=0.19 ^{+0.11} _{-0.06}	4/21=0.19 ^{+0.11} _{-0.06}
F4–G2	1.4–1.5	1/25=0.04 ^{+0.08} _{-0.01}	1/8=0.12 ^{+0.20} _{-0.04}	1/25=0.04 ^{+0.08} _{-0.01}	1/25=0.04 ^{+0.08} _{-0.01}
G2–K0	1.3–1.4	1/19=0.05 ^{+0.10} _{-0.02}	1/10=0.10 ^{+0.17} _{-0.03}	1/18=0.06 ^{+0.11} _{-0.02}	1/19=0.05 ^{+0.10} _{-0.02}
K0–M0	0.7–1.3	22/158=0.14 ^{+0.03} _{-0.02}	9/54=0.17 ^{+0.06} _{-0.04}	26/157=0.17 ^{+0.03} _{-0.02}	26/156=0.17 ± 0.03
M0–M4	0.2–0.7	86/563=0.15 ± 0.02	21/127=0.17 ^{+0.04} _{-0.03}	97/537=0.18 ± 0.02	38/178=0.21 ± 0.03
M4–M8	0.035–0.2	203/1036=0.20 ± 0.01	27/116=0.23 ^{+0.04} _{-0.03}
M8–L2	0.01–0.035	27/115=0.23 ^{+0.04} _{-0.03}
Debris and Evolved Transitional Disks					
B0–B8	2.8–18	0/21=<0.08	0/18=<0.09	1/22=0.05 ^{+0.09} _{-0.01}	0/23=<0.07
B8–A6	1.8–2.8	0/47=<0.04	1/29=0.03 ^{+0.07} _{-0.01}	9/49=0.18 ^{+0.07} _{-0.04}	22/49=0.45 ± 0.07
A6–F4	1.5–1.8	1/17=0.06 ^{+0.11} _{-0.02}	0/5=<0.27	3/21=0.14 ^{+0.11} _{-0.04}	11/21=0.52 ± 0.10
F4–G2	1.4–1.5	0/25=<0.07	0/8=<0.19	1/25=0.04 ^{+0.08} _{-0.01}	10/25=0.40 ^{+0.10} _{-0.08}
G2–K0	1.3–1.4	0/19=<0.09	0/10=<0.16	0/18=<0.09	2/19=0.11 ^{+0.11} _{-0.03}
K0–M0	0.7–1.3	3/158=0.02 ^{+0.02} _{-0.01}	0/54=<0.03	4/157=0.03 ^{+0.02} _{-0.01}	16/156=0.10 ^{+0.03} _{-0.02}
M0–M4	0.2–0.7	1/563=0.002 ^{+0.004} _{-0.001}	0/127=<0.01	13/537=0.02 ± 0.01	26/178=0.15 ^{+0.03} _{-0.02}
M4–M8	0.035–0.2	2/1036=0.002 ^{+0.002} _{-0.001}	2/116=0.02 ^{+0.02} _{-0.01}
M8–L2	0.01–0.035	0/115=<0.02

^a Masses that correspond to the given range of spectral types for an age of 10 Myr (Baraffe et al. 1998, 2015; Choi et al. 2016; Dotter 2016).

TABLE 7
DISK FRACTION FOR UPPER SCO

Spectral Type	N(primitive disks)/N(all stars)
<K6	20/174=0.11 ^{+0.03} _{-0.02}
K6-M3.5	84/515=0.16 ± 0.02
M3.75-M5.75	215/966=0.22 ± 0.02
M6-M8	51/228=0.22 ± 0.03
>M8-M9.75	27/107=0.25 ^{+0.05} _{-0.04}

TABLE 8
PARAMETERS FOR EXTINCTION COEFFICIENTS IN *Gaia* BANDS^a

	c_1	c_2	c_3	c_4	c_5	c_6	c_7	c_8	c_9
$k_{G,5500}$	0.9605	-0.1355	-0.03399	0.00532	0.00847	0.001217	0.000464	-0.0000199	-0.0000257
$k_{G,V}$	0.9536	-0.1145	-0.03211	0.00554	0.00000	0.001242	0.001398	-0.0000208	-0.0000235
$k_{BP,5500}$	1.1522	-0.1150	-0.02237	0.00296	0.02487	0.000730	-0.001754	-0.0000097	-0.0000197
$k_{BP,V}$	1.1425	-0.0900	-0.01960	0.00322	0.01663	0.000797	-0.001016	-0.0000104	-0.0000142
$k_{RP,5500}$	0.6389	-0.0189	-0.00782	0.00075	-0.00744	0.000081	0.001150	0.0000002	-0.0000001
$k_{RP,V}$	0.6309	-0.0005	-0.00540	0.00060	-0.01363	0.000045	0.001724	0.0000014	0.0000073

^a $k_{\lambda_1, \lambda_2} = A_{\lambda_1}/A_{\lambda_2} = c_1 + c_2(G_{BP} - G_{RP}) + c_3 A_{\lambda_2} + c_4(G_{BP} - G_{RP})A_{\lambda_2} + c_5(G_{BP} - G_{RP})^2 + c_6 A_{\lambda_2}^2 + c_7(G_{BP} - G_{RP})^3 + c_8 A_{\lambda_2}^3 + c_9(G_{BP} - G_{RP})^2 A_{\lambda_2}^2$ where $G_{BP} - G_{RP}$ is the intrinsic color. These coefficients are based on the extinction curve from Schlafly et al. (2016) for $x = 0$ ($R_V \approx 3.3$) and are valid for stars with intrinsic colors of $G_{BP} - G_{RP} \sim 0-4.4$ mag and $A_V \leq 20$ mag and $A_{5500} \leq 20$ mag.

TABLE 9
INTRINSIC COLORS OF YOUNG STARS AND BROWN DWARFS

Column Label	Description
SpType	Spectral Type
BP-RP	$G_{\text{BP}} - G_{\text{RP}}$ for <i>Gaia</i> DR2 bands
G-RP	$G - G_{\text{RP}}$ for <i>Gaia</i> DR2 bands
RP-K	$G_{\text{RP}} - K_s$ for <i>Gaia</i> DR2 and 2MASS bands
J-H	$J - H$ for 2MASS bands
H-K	$H - K_s$ for 2MASS bands
K-3.6	$K_s - [3.6]$ for 2MASS and <i>Spitzer</i> bands
K-4.5	$K_s - [4.5]$ for 2MASS and <i>Spitzer</i> bands ^a
K-5.8	$K_s - [5.8]$ for 2MASS and <i>Spitzer</i> bands
K-8.0	$K_s - [8.0]$ for 2MASS and <i>Spitzer</i> bands
K-24	$K_s - [24]$ for 2MASS and <i>Spitzer</i> bands ^b
K-W1	$K_s - W1$ for 2MASS and <i>WISE</i> bands
K-W2	$K_s - W2$ for 2MASS and <i>WISE</i> bands ^a
K-W3	$K_s - W3$ for 2MASS and <i>WISE</i> bands
K-W4	$K_s - W4$ for 2MASS and <i>WISE</i> bands ^b

NOTE. — The table is available in its entirety in machine-readable form.

^a Same values listed for $K_s - [4.5]$ and $K_s - W2$.

^b Same values listed for $K_s - [24]$ and $K_s - W4$.

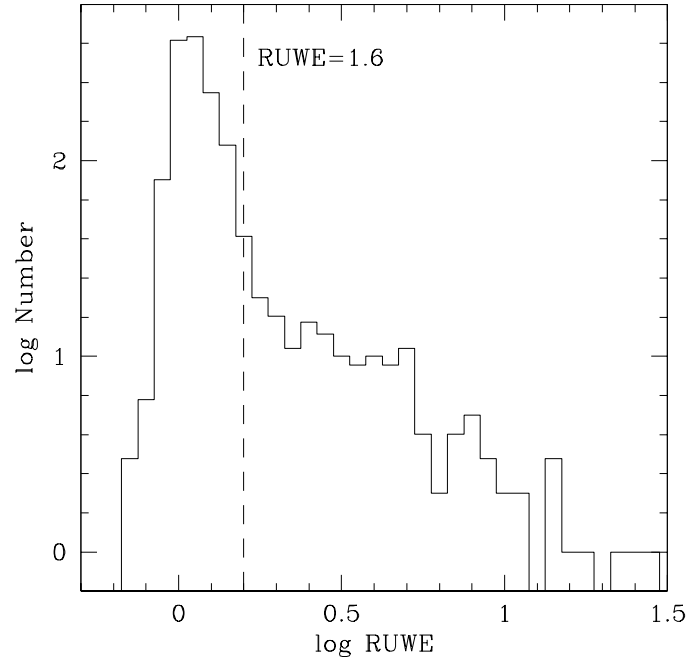


FIG. 1.— Distribution of $\log(\text{RUWE})$ for stars adopted as members of the Upper Sco association by Luhman et al. (2018) that have parallax measurements from *Gaia* DR2 (histogram). RUWE characterizes the quality of the astrometric fit for a given star (Lindgren 2018). We treat astrometry for stars with $\text{RUWE} < 1.6$ as reliable.

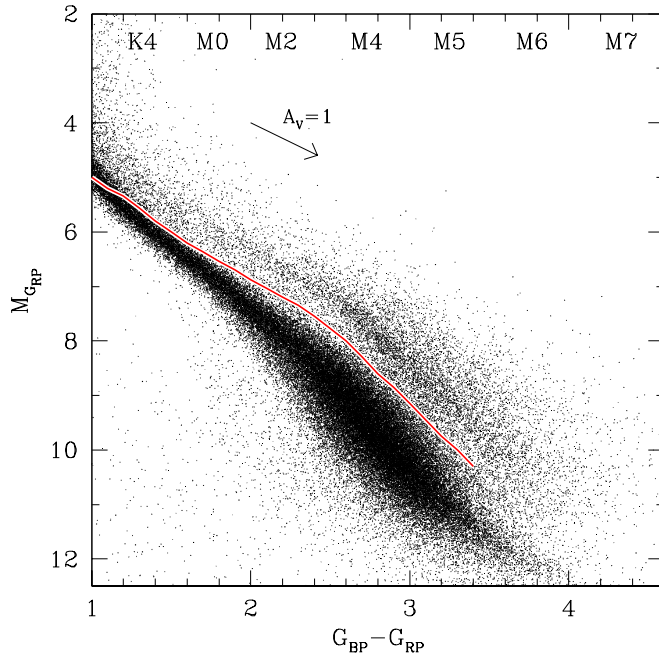


FIG. 2.— $M_{G_{\text{RP}}}$ versus $G_{\text{BP}} - G_{\text{RP}}$ for stars within the boundary of Sco-Cen defined by de Zeeuw et al. (1999) that have $\pi > 5$ mas, $\pi/\sigma \geq 20$, and $\text{RUWE} < 1.6$ in *Gaia* DR2. We have selected a sample of candidate young low-mass stars based on colors of $G_{\text{BP}} - G_{\text{RP}} = 1.4$ – 3.4 mag (~ 0.15 – $1 M_{\odot}$) and positions above the single-star sequence for the Tuc-Hor association (45 Myr, Bell et al. 2015) (solid line). We have marked a reddening vector for the extinction curve from Schlafly et al. (2016) and the spectral types that correspond to these colors for young stars (see Appendix).

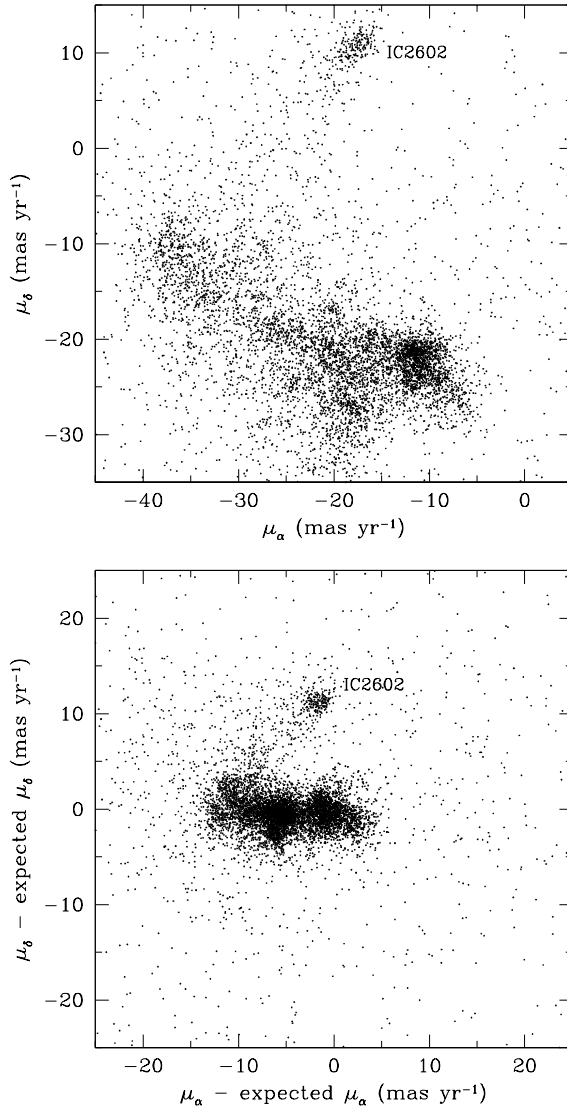


FIG. 3.— Proper motions and proper motion offsets for candidate young stars within the boundaries of Sco-Cen selected from Figure 2. The offsets are computed relative to the proper motions expected for the positions and parallaxes assuming the median space velocity of Upper Sco members ($U, V, W = -5, -16, -7$ km s⁻¹, Section 4).

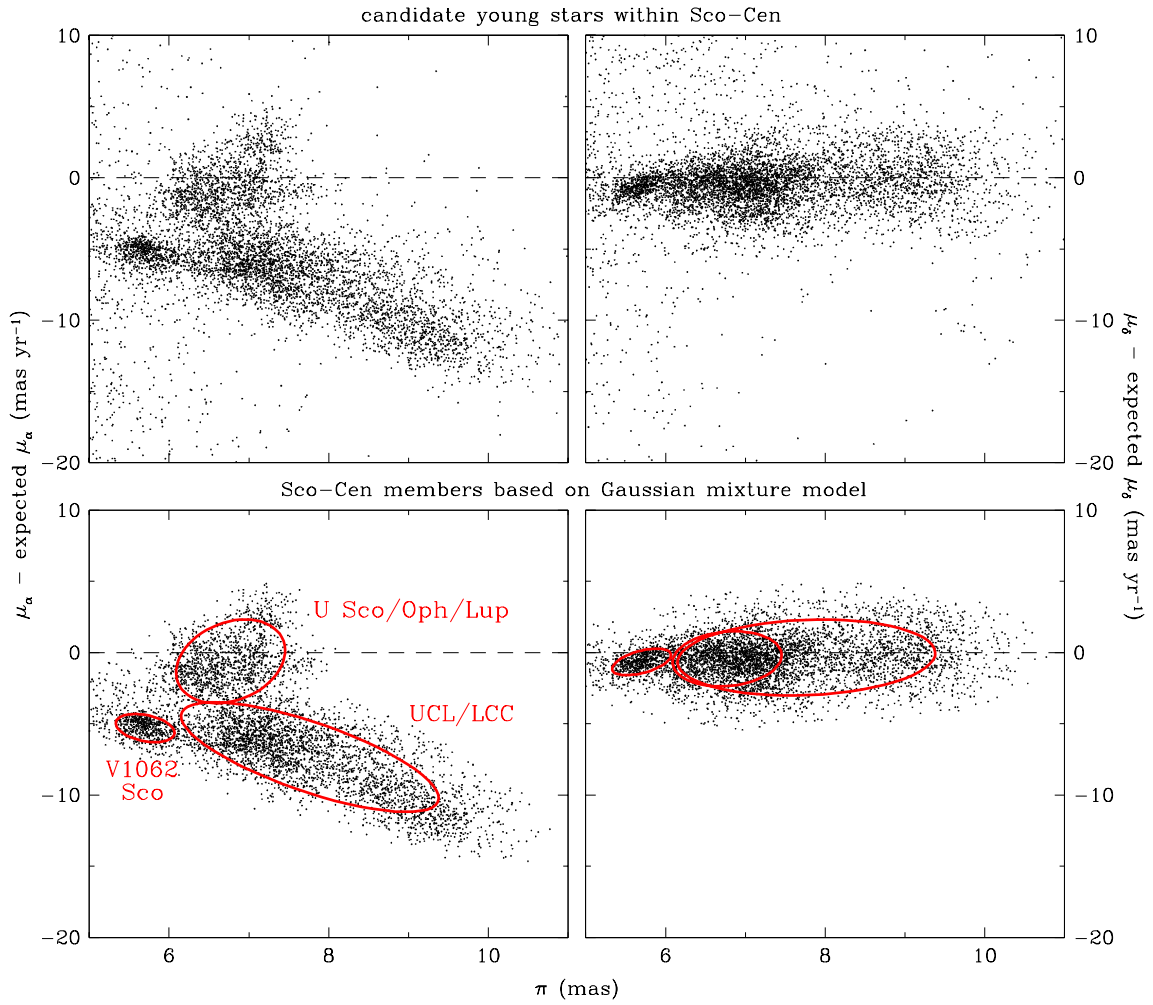


FIG. 4.— Proper motion offsets versus parallax for candidate young stars within the boundaries of Sco-Cen selected from Figure 2 (top). A Gaussian mixture model has been applied to these data to estimate probabilities of membership in Sco-Cen and the field population. The stars that have $> 90\%$ probabilities of membership in Sco-Cen are shown (bottom). The three Sco-Cen components in the model are represented by the ellipses (2σ).

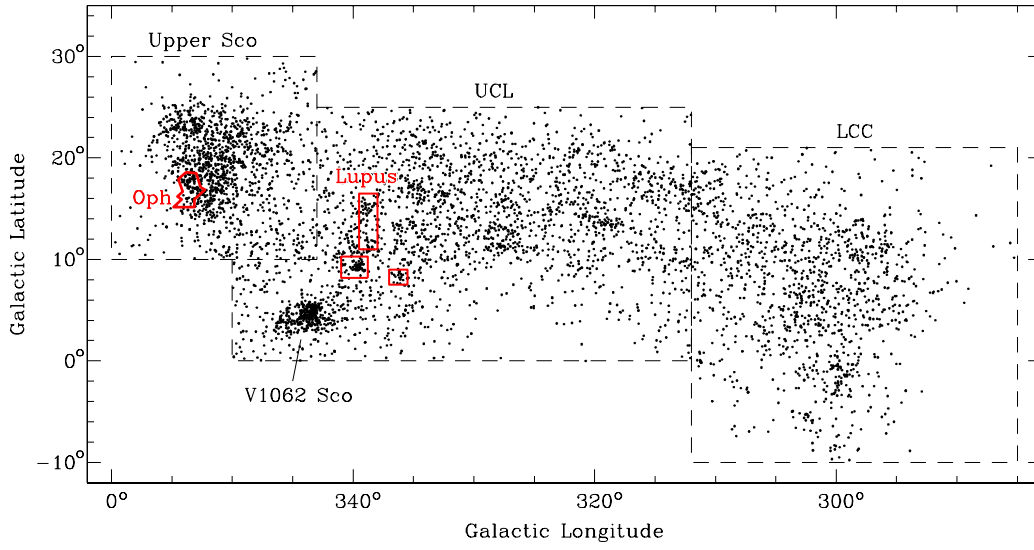


FIG. 5.— Spatial distribution of the candidate members of Sco-Cen with $> 90\%$ membership probabilities from Figure 4. The boundaries from de Zeeuw et al. (1999) for the subgroups are indicated (dashed lines). We also have marked the boundary between Upper Sco and Ophiuchus from Esplin et al. (2018) and rectangles that encompass clouds 1–4 in Lupus (solid red lines).

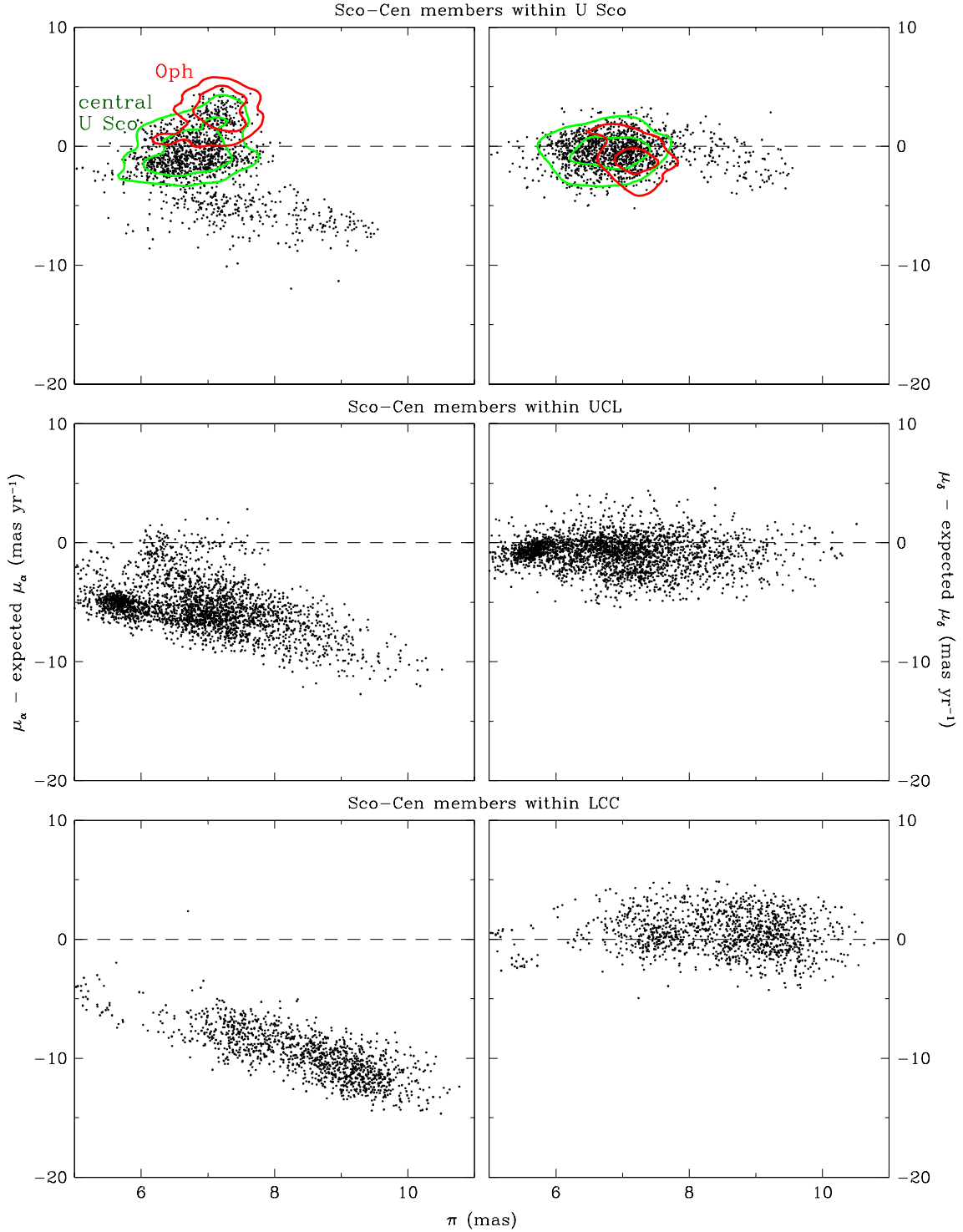


FIG. 6.— Proper motion offsets versus parallax for the candidate members of Sco-Cen with $> 90\%$ membership probabilities (Figure 4) that are within the boundaries of Upper Sco (top), UCL (middle), and LCC (bottom) from de Zeeuw et al. (1999). We have included contours for density maps of the data within the central concentration in Upper Sco and within the boundary of Ophiuchus from Esplin et al. (2018) (see Fig. 5). For each of those populations, the contours are plotted at 10% and 50% of the maximum density.

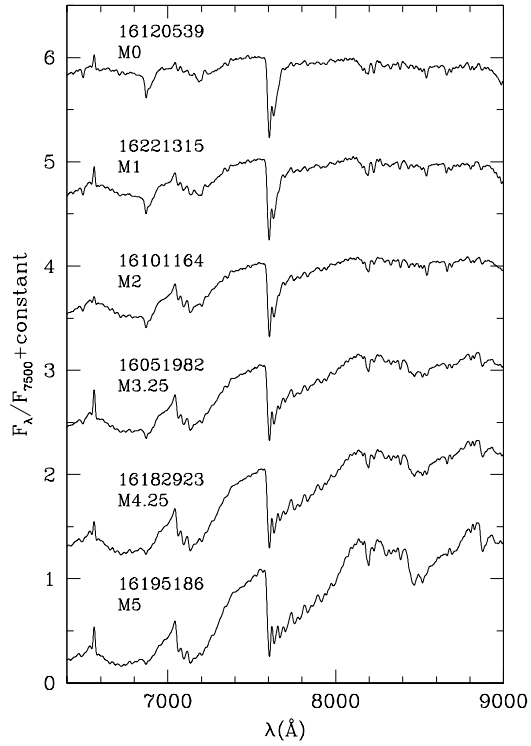


FIG. 7.— Examples of optical spectra of members of the Upper Sco association. These data are displayed at a resolution of 13 \AA . The data used to create this figure are available.

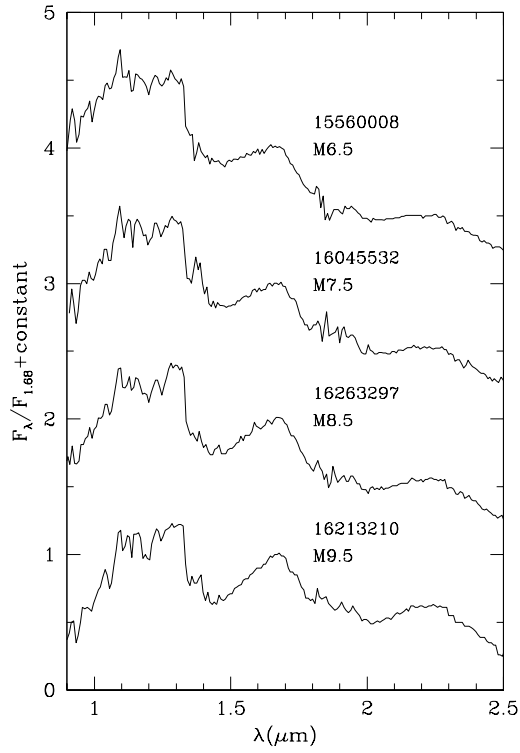


FIG. 8.— Examples of near-IR spectra of M-type members of the Upper Sco association. They have been dereddened to match the slopes of the young standards from Luhman et al. (2017) and are displayed at a resolution of $R = 200$. The data used to create this figure are available.

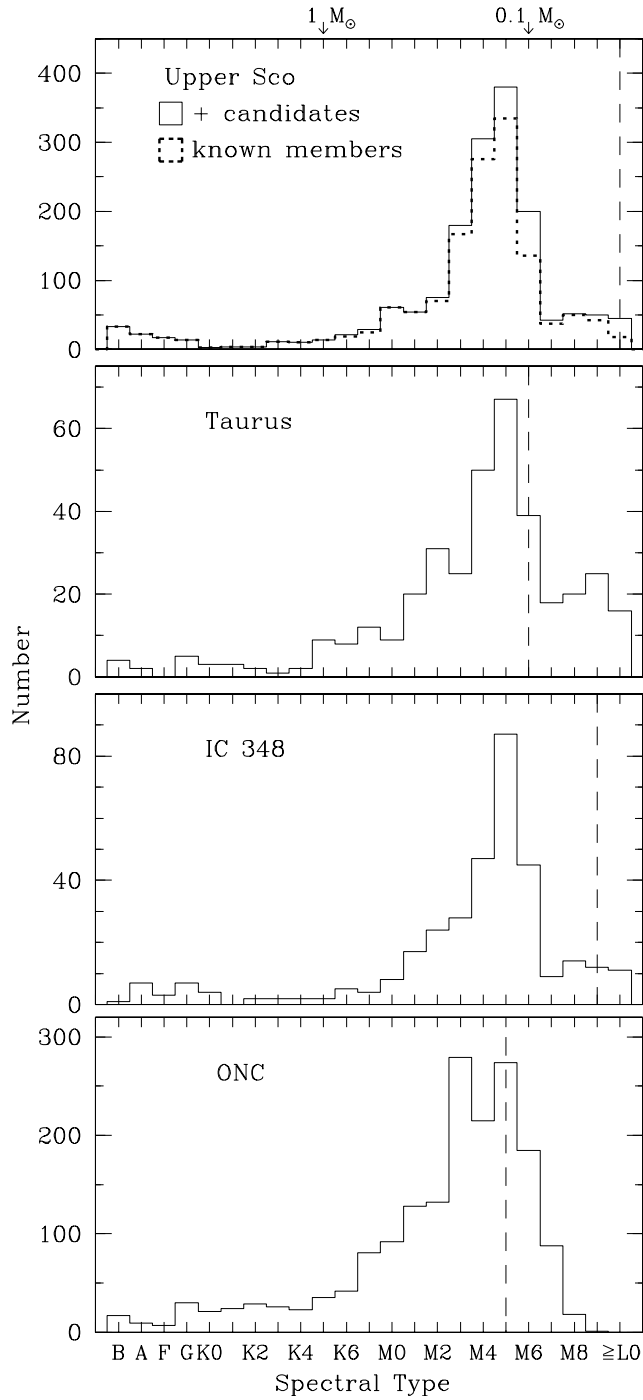


FIG. 9.— Distributions of spectral types for the central concentration in Upper Sco (Figure 5), Taurus ($A_J < 1$ mag, Esplin & Luhman 2019), IC 348 ($A_J < 1.5$ mag, Luhman et al. 2016), and the ONC (Da Rio et al. 2012; Hillenbrand et al. 2013). We also show the distribution for Upper Sco after including candidate members that lack confirmation of youth (Table 1). The dashed lines indicate the completeness limits of these samples and the arrows mark the spectral types that correspond to masses of $0.1 M_{\odot}$ and $1 M_{\odot}$ for ages of a few Myr according to evolutionary models (e.g., Baraffe et al. 1998).

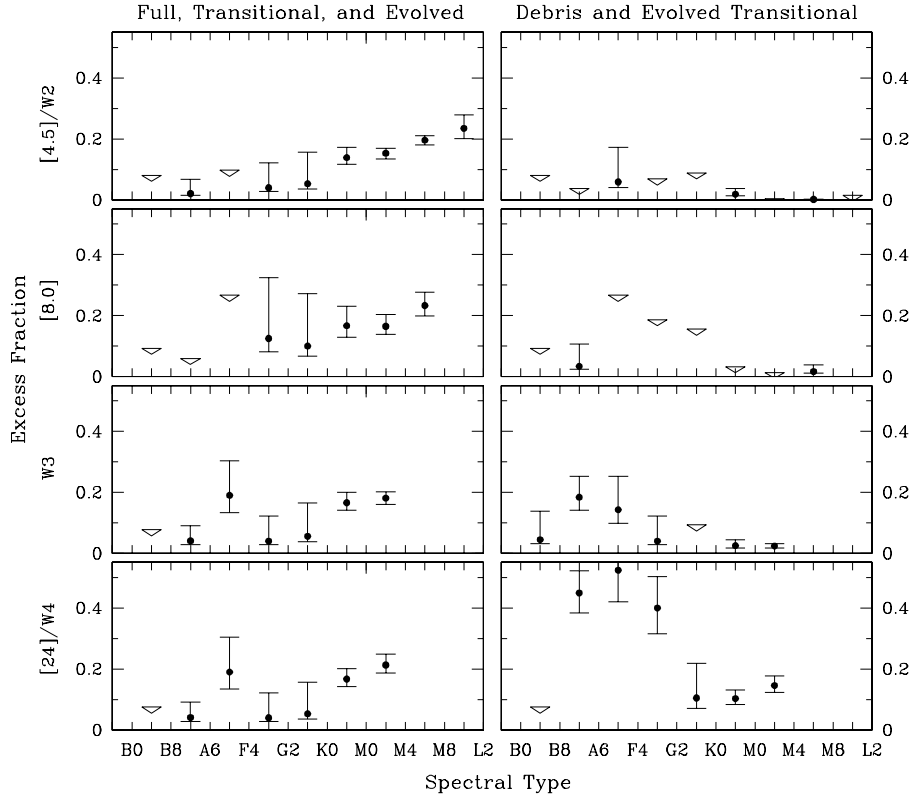


FIG. 10.— Excess fractions versus spectral type in Upper Sco for full, transitional, and evolved disks (left) and debris and evolved transitional disks (right, Table 6). For each band, data are shown only down to the coolest spectral type at which most of the known members are detected. The triangles represent 1σ upper limits.

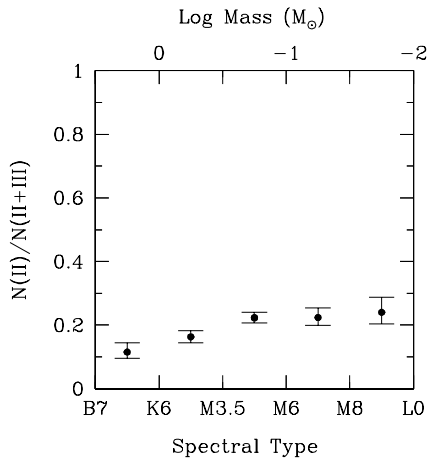


FIG. 11.— Fraction of Upper Sco members with primordial disks (full, transitional, evolved) as a function of spectral type (Table 7). The boundaries of the spectral type bins were chosen to correspond approximately to logarithmic intervals of mass.

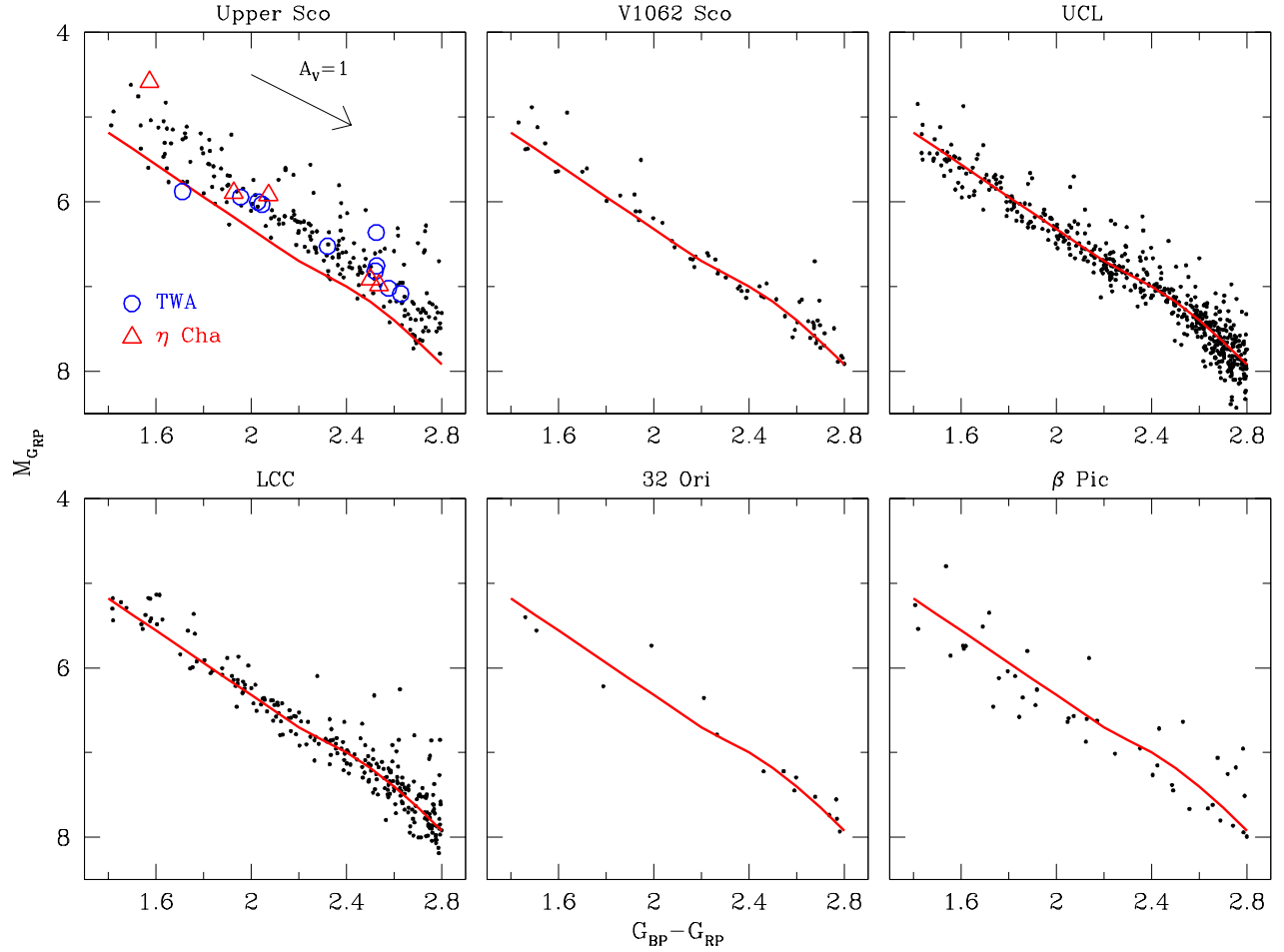


FIG. 12.— $M_{G_{\text{RP}}}$ versus $G_{\text{BP}} - G_{\text{RP}}$ for low-mass diskless stars ($\sim 0.2-1 M_{\odot}$) in populations within Sco-Cen and in the 32 Ori association (Bell et al. 2017) and the β Pic moving group (Bell et al. 2015; Gagné et al. 2018). A fit to the median of the combined sequence for UCL and LCC is shown with each sample (red solid line). TWA (Gagné et al. 2017) and η Cha (Luhman & Steeghs 2004; Lyo et al. 2004) are also plotted with Upper Sco to illustrate the similarity in their ages.

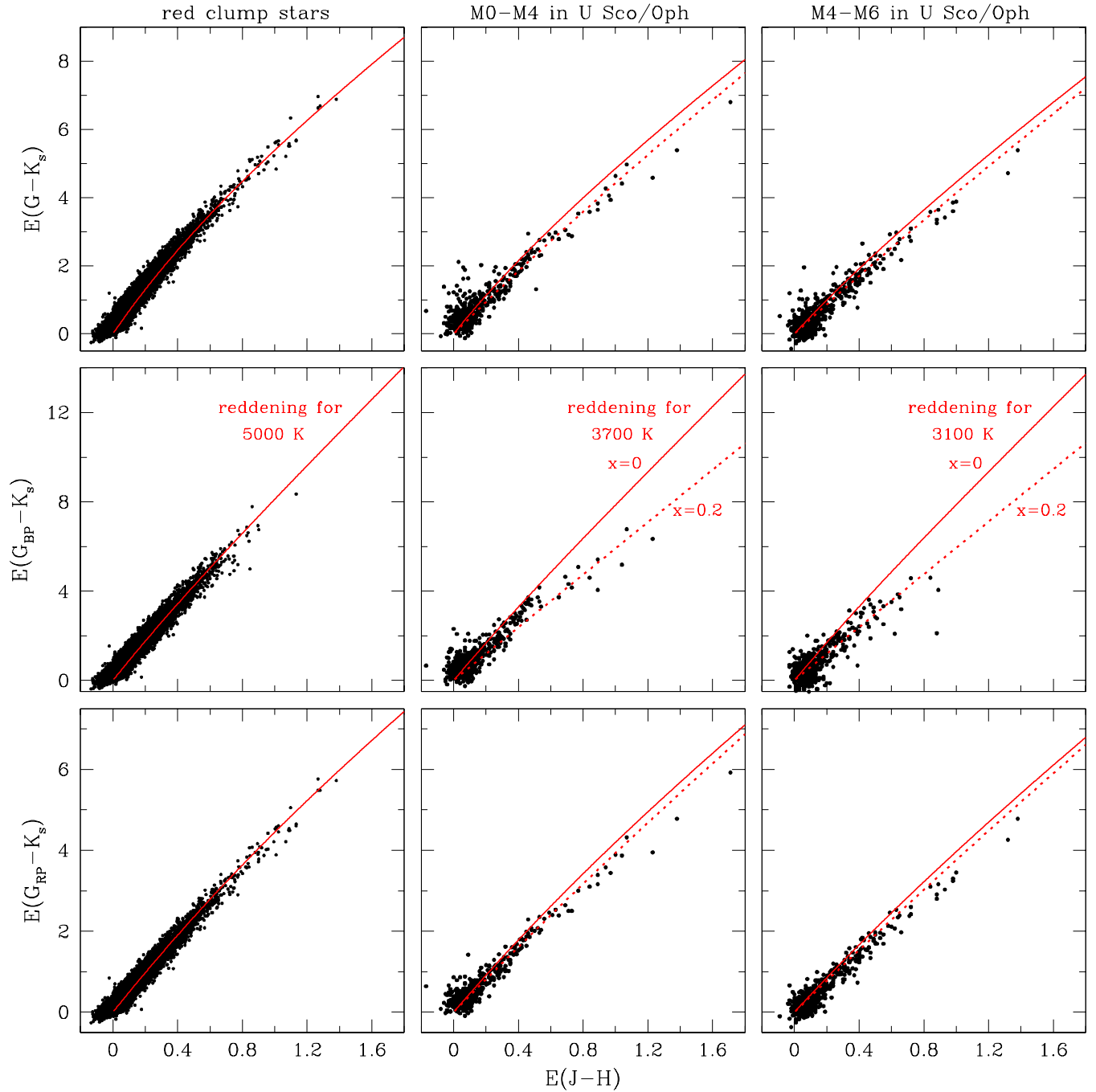


FIG. 13.— Color excesses in the *Gaia* bands relative to K_s versus excesses in $J-H$ for red clump stars from APOGEE (left) and stars in Upper Sco and Ophiuchus with spectral types of M0–M4 and M4–M6 that lack excess emission from disks at $< 5 \mu\text{m}$ (middle and right). The solid lines represent reddening vectors produced by the extinction curve from Schlafly et al. (2016) for $x = 0$ ($R_V \approx 3.3$) and model spectra with intrinsic $G_{BP} - G_{RP}$ colors that are similar to those of each sample. For the young stars, we also include vectors for $x = 0.2$ ($R_V \approx 5$, dotted lines).